Classification-- BIOLOGICAL SCIENCES: Biochemistry

Structural and molecular basis of the assembly of the TRPP2/PKD1 complex

Yong Yu[a], Maximilian H. Ulbrich[b], Ming-hui Li[a], Zafir Buraei[a], Xing-Zhen Chen[d], Albert C.M. Ong[e], Liang Tong[a], Ehud Y. Isacoff[b,c] and Jian Yang[a, 1]

[a]Department of Biological Sciences, Columbia University, New York, NY 10027, USA

[b]Department of Molecular and Cell Biology, University of California, Berkeley, CA 94720, USA

[c]Material Sciences & Physics Biosciences Divisions, Lawrence Berkeley National Laboratory, Berkeley, CA 94720, USA

[d]Membrane Protein Research Group, Department of Physiology, Faculty of Medicine and Dentistry, University of Alberta, Edmonton, Alberta, T6G 2H7, Canada

[e]Kidney Genetics Group, Academic Unit of Nephrology, Sheffield Kidney Institute, School of Medicine and Biomedical Sciences, University of Sheffield, Sheffield, UK

[1] To whom correspondence should be addressed.

Jian Yang

Department of Biological Sciences, 917 Fairchild Center, MC2462, Columbia University, New York, NY 10027

Phone: (212)-854-6161; Fax: (212)-531-0425 Email: jy160@columbia.edu

Author contributions: Y.Y., M.H.U., M.L., Z.B., X-Z.C., A.C.M.O, L.T., E.Y.I., and J.Y. designed research; Y.Y., M.H.U., M.L., and Z.B. preformed research; Y.Y., M.H.U., Z.B. and J.Y. analyzed data; and Y.Y., M.H.U, E.Y.I. and J.Y. wrote the paper.

Manuscript information: 27 text pages and 5 figures.

Data deposition: The atomic coordinates and structure factors have been deposited in Protein Data Bank, www.pdb.org (PDB ID codes).

Abstract

Mutations in PKD1 and TRPP2 account for nearly all cases of autosomal dominant polycystic kidney disease (ADPKD). These two proteins form a receptor/ion channel complex on the cell surface. Using a combination of biochemistry, crystallography and a single molecule method to determine the subunit composition of proteins in the plasma membrane of live cells, we find that this complex contains 3 TRPP2 and 1 PKD1. A newly identified coiled coil domain in the C terminus of TRPP2 is critical for the formation of this complex. This coiled coil domain forms a homotrimer, both in solution and in crystal structure, and binds to a single coiled coil domain in the C terminus of PKD1. Mutations that disrupt the TRPP2 coiled coil domain trimer abolish the assembly of both the full-length TRPP2 trimer and the TRPP2/PKD1 complex, and diminish the surface expression of both proteins. These results have significant implications for the assembly, regulation and function of the TRPP2/PKD1 complex, and for the pathogenic mechanism of some ADPKD-producing mutations.

\body

Autosomal dominant polycystic kidney disease (ADPKD), one of the most common genetic diseases in humans, is caused by mutations in PKD1 or TRPP2 (1-3). PKD1 (also known as polycystin-1 or PC1) is a 4302-amino acid (aa), 465 kDa integral membrane protein containing 11 putative transmembrane regions (4) (Fig. S1). Its large extracellular N terminus contains a number of well

recognized repeats and domains, some of which are known to interact with extracellular matrix proteins. The short intracellular C terminus contains a G protein activation site. Thus, PKD1 is generally thought to function as a cell surface receptor for extracellular ligands and matrix proteins that couples extracellular stimuli, including mechanical stimuli, to intracellular signaling (1, 4-6). TRPP2 (also known as PKD2, polycystin-2 or PC2) is a member of the transient receptor potential (TRP) channel family (7). TRPP2 is a 968-aa, 110 kDa integral membrane protein with 6 putative transmembrane segments and a pore-forming loop (7) (Fig. S1) and forms a Ca^{2+}-permeable nonselective cation channel (8-10).

How mutations in PKD1 and TRPP2 lead to ADPKD is unclear. The two proteins likely participate in the same molecular and cellular processes in some kidney cells, since their mutations produce similar pathological manifestations. Although both proteins are widely distributed, they show high levels of expression in kidney cells (1, 5-7), where they are present on the plasma membrane and in the Golgi and endoplasmic reticulum (1, 4-6, 11-13). They also colocalize in the primary cilia of kidney epithelium (14). The two proteins associate physically (15-19) and form functional complexes (18, 20, 21). However, the subunit composition of this heteromeric complex and the molecular mechanism underlying its assembly are unknown.

In this work we investigated these issues using a multifaceted approach that includes biochemistry, x-ray crystallography and single molecule optical

imaging. Our study provides the structural basis of the homomeric assembly of a functionally important TRPP2 coiled coil domain, uncovers the crucial role of this domain in the assembly of the TRPP2/PKD1 complex, and reveals an unexpected subunit stoichiometry of this complex.

Results

Subunit stoichiometry of the TRPP2 homomultimer expressed in a cell line. To study the molecular mechanism of the assembly of the TRPP2/PKD1 complex, we first examined the stoichiometry of the TRPP2 complex in the absence of PKD1. TRPP2 purified from a HEK 293T cell line stably expressing HA-TRPP2 [TRPP2 tagged with hemagglutinin (HA) on the N terminus] was analyzed by blue native polyacrylamide gel electrophoresis (BN-PAGE). Undenatured and unreduced TRPP2 protein migrated as a complex with an apparent molecular weight (M.W.) of ~850 kDa (Fig. 1*A*, lane 1). Denatured and reduced protein migrated as a complex with an apparent M.W. of ~280 kDa (Fig. 1*A*, lane 2). In contrast, denatured but unreduced protein showed three products, with an apparent M.W. of ~280 kDa, ~600 kDa, and ~850 kDa (Fig. 1*A*, lane 3). The relative size of the three products suggests that they correspond to the TRPP2 monomer, dimer and trimer. The apparent M.W. of these products is much larger than their predicted M.W. (110 kDa, 220 kDa, and 330 kDa, respectively). Glycosylation, detergent binding, and/or anomalous mobility in BN-PAGE probably account for their much higher observed M.W.

We next used chemical cross-linking to further determine the subunit stoichiometry of the TRPP2 homomeric complex. Treatment of the lysate of the HA-TRPP2-expressing cells with the amine-reactive cross-linker DST resulted in three products, with an apparent M.W. of 120 kDa, 260 kDa and 400 kDa (Fig. 1*B*), which likely correspond to the TRPP2 monomer, dimer and trimer (the largest band is unlikely to be the tetramer since the extrapolated M.W. of the tetramer would be ~520 kDa). These and the preceding results indicate that the prevalent form of TRPP2 in the cell lysate is a trimer.

We also produced two other HEK 293T stable lines, expressing either FLAG-PKD1 (PKD1 tagged with FLAG on the N terminus) or FLAG-PKD1 plus HA-TRPP2. Due to technical challenges, our attempts to cross-link TRPP2 and PKD1 produced inconclusive results (data not shown).

Subunit stoichiometry of the TRPP2/PKD1 heteromeric and TRPP2 homomeric complex in the membrane of live cells. Next, we used a single molecule optical approach (22) to determine the stoichiometry of the TRPP2/PKD1 complex as well as the homomeric TRPP2 complex in the membrane of live cells. This method uses total internal reflection fluorescence (TIRF) microscopy to visualize single, GFP-tagged proteins exclusively on the plasma membrane of *Xenopus* oocytes. Measurements were made simultaneously for many complexes at low levels of protein expression, where the formation of non-native high-order complexes and aggregates is avoided.

The number of GFP photobleaching steps was used to determine the number of subunits of one of the proteins in a complex and a mCherry tag was used to reveal the presence of the second subunit type within the same complex.

We fused EGFP or mCherry to the cytosolic C terminus of TRPP2 or PKD1 (the resultant subunits were named TRPP2-EGFP, TRPP2-mCherry, PKD1-EGFP and PKD1-mCherry). *Xenopus* oocytes were injected with the cRNAs of PKD1-mCherry and TRPP2-EGFP, or of PKD1-EGFP and TRPP2-mCherry. Surface fluorescent spots were visualized by first exciting mCherry and then EGFP. Spots showing dual fluorescence were identified as TRPP2/PKD1 complexes (Fig. 1 *C* and *F*). Although many spots diffused laterally in the membrane, a large portion (~40%) was immobile and their EGFP bleaching steps could be counted (e.g. circle spots in Fig. 1 *C* and *F*). In oocytes expressing PKD1-mCherry and TRPP2-EGFP, most dual-fluorescence spots showed 2 or 3 EGFP bleaching steps, with a small minority of the spots bleaching in 1 or 4 steps (Fig. 1 *D* and *E*). The 1-3 step distribution is well fit by a binomial distribution (Fig. 1*E*) that assumes that each spot contains 3 EGFPs and that the probability of EGFP to be fluorescent is 83%, similar to what was observed earlier on other membrane proteins (22). The presence of a small number of spots (3.5% of the dual-fluorescence spots) that showed 4 EGFP bleaching steps can be accounted for by the occasional colocalization of two complexes. The distribution of EGFP bleaching steps fits poorly to a binomial distribution that assumes that each spot contains 4 EGFPs (Fig. S2). In the

complementary experiment in oocytes expressing PKD1-EGFP and TRPP2-mCherry (Fig. 1*F*), most dual-fluorescence spots showed only 1 EGFP bleaching step (Fig. 1 *G* and *H*). A small minority of spots showed 2 EGFP bleaching steps (Fig. 1*H*), probably because they contained two complexes. mCherry showed a gradual decrease in fluorescence, indicating the presence of several subunits (Fig. 1*G*), but due to mCherry's weak fluorescence emission and large fluorescence fluctuations, steps could not be counted reliably. Taken together, these results indicate that the TRPP2/PKD1 full channel complex on the surface membrane of *Xenopus* oocytes contains 3 TRPP2 and 1 PKD1.

Numerous PKD1 fluorescence spots were observed on the plasma membrane of oocytes expressing PKD1-EGFP and TRPP2-mCherry (Fig. 1*F* and Fig. S3*A*); however, very few spots were observed in oocytes expressing PKD1-EGFP alone (Fig. S3*B*). This indicates that, on its own, PKD1 reaches the surface membrane very inefficiently. In contrast, abundant fluorescence spots were detected on the plasma membrane of oocytes expressing TRPP2-EGFP alone (Fig. S3*C*). This suggests that TRPP2 reaches the surface membrane either on its own or, perhaps, in complex with an unknown endogenous oocyte protein. One such candidate protein is TRPC1, which is endogenously expressed in oocytes (23) and directly associates with TRPP2 (17, 21, 24). Fluorescence spots from oocytes expressing TRPP2-EGFP alone showed the same EGFP bleaching pattern (Fig. S3 *D* and *E*) as did the dual-fluorescence spots from oocytes expressing TRPP2-EGFP and PKD1-mCherry (Fig. 1 *D* and

E), indicating that the complex containing TRPP2-EGFP alone has 3 subunits of TRPP2. This is in agreement with the stoichiometry of the TRPP2 homomeric complex in HEK 293 cell lysates determined biochemically (Fig. 1 *A* and *B*).

Stoichiometry of a TRPP2/PKD1 C terminal coiled coil domain complex. We next investigated the molecular basis for the 3:1 stochiometry of the TRPP2/PKD1 complex. Previous studies show that C terminal fragments of TRPP2 and PKD1 associate with each other *in vitro* (15-17). The interaction site has been mapped to amino acids H822 to G895 in TRPP2 (17) and a putative coiled coil domain (L4214 to R4248) in PKD1 (15). We examined the stoichiometry of complexes formed by TRPP2 and PKD1 C terminal fragments encompassing these regions, which were co-expressed in and co-purified from bacteria. The measured M.W. of these complexes, determined by static light scattering (Fig. S4), closely matches the predicted M.W. of 3 TRPP2 and 1 PKD1 (Fig. 2, bars 1 and 2). Likewise, the measured M.W. of two different TRPP2 fragments corresponds nicely with the calculated M.W. of 3 TRPP2 (Fig. 2 bars 3 and 4). These results indicate that the C terminal domain of TRPP2 forms a homotrimer and that this trimer can associate with the C terminus of one PKD1 to form a 3:1 complex.

Crystal structure a TRPP2 C terminal coiled coil domain. To examine how the TRPP2 C terminal domain forms a homotrimer, we solved the crystal

structure of a C terminal fragment of TRPP2 harboring the PKD1 coiled coil domain-interaction site. This fragment, from amino acid G833 to G895, is conserved across species (Fig. 3*A*) and contains a predicted coiled coil domain (from F839 to A873) (Fig. 3*B*). The structure, solved at 1.9 Å resolution (Fig. 3*C*, Table S1, and Fig. S5), shows that this fragment forms a continuous α helix (from Y836 on) and assembles into a trimer. The N terminal portion containing the coiled coil domain (from Y836 to R872) is tightly bundled together via extensive hydrophobic interactions (Fig. 3*D*). The C terminal portion of the α helices, from A873 to G895, splays open (Fig. 3*C*). In the crystal lattice, this region interacts with the same region of another trimer, forming a hexameric complex containing two interacting trimers (Fig. 3*E*). This hexameric complex is likely the result of construct design and crystal packing since, in solution, longer TRPP2 fragments encompassing the aforementioned α helix clearly form a trimer, not a hexamer (Fig. 2, bars 3 and 4).

We also solved the structure of a fragment (from G833 to R872) containing only the coiled coil domain (Fig. 3*F* and Table S1). Superposition of this structure with that of the longer fragment shows a high degree of overlap (Fig. 3*G*), with an r.m.s.d of 0.55 Å when the Cα atoms of the coiled coil are superimposed. This indicates that the C terminal interaction observed in the crystal between two trimers (Fig. 3*E*) did not perturb the structure of the coiled coil domain.

Disruption of the TRPP2 coiled coil domain trimer abolishes TRPP2/PKD1 coiled coil domain interaction. Pull-down experiments showed that the TRPP2 G833-G895 fragment, tagged with small ubiquitin-like modifier (SUMO), was able to bind the maltose binding protein (MBP)-tagged PKD1 coiled coil domain, MBP-PKD1_R4213–R4248 (Fig. 4*A*, lane 1). However, neither the trimer-forming "bundled" TRPP2_G833–R872 fragment nor the downstream "open" E871-G895 fragment could, on its own, interact with the PKD1 coiled coil domain (Fig. 4*A*, lanes 2 and 3). Indeed, even TRPP2_V857-G895, which contains more than one third of the trimer-forming residues as well as the "open" region, could not bind the PKD1 fragment (Fig. 4*A*, lane 4). Thus, the TRPP2/PKD1 coiled coil domain interaction requires both the "bundled" and "open" regions of TRPP2. The physical/chemical nature of this interaction remains to be elucidated.

We next tested whether the TRPP2 coiled coil domain trimer was necessary for forming the TRPP2/PKD1 (3:1) C terminal complex. Six hydrophobic residues (L842, V846, M849, I860, V863 and L867, Fig. 3*D*) critical for forming the trimer were simultaneously mutated to alanine in an MBP-tagged TRPP2 C terminal fragment, MBP-TRPP2_G821-S926 (this hexa-alanine mutation was named "mut6"). Gel filtration profile and static light scattering both indicated that this mut6 fragment did not form a trimer; instead, it remained as a monomer (Fig. 4*B*). Pull-down experiments showed that a slightly shorter TRPP2 fragment (G833-S918) carrying mut6 could not bind the PKD1 coiled coil domain (R4213-R4248), while the corresponding wild-type (WT) TRPP2

fragment was fully competent (Fig. 4*C*). These results indicate that the PKD1 coiled coil domain binds the TRPP2 trimer but does not bind the TRPP2 monomer.

Disruption of the TRPP2 coiled coil domain trimer disrupts the assembly of the full length TRPP2/PKD1 complex. To further examine the functional importance of the TRPP2 coiled coil domain trimer, we engineered the mut6 mutation into full-length TRPP2 and created two additional HEK 293T stable cell lines, expressing either HA-TRPP2_mut6 or HA-TRPP2_mut6 plus FLAG-PKD1. Two lines of evidence demonstrate that full-length TRPP2_mut6 do not interact with each other to form homomeric complexes: (i) TRPP2_mut6 could not be cross-linked (Fig. 5*A*). Cross-linking of WT TRPP2 with DST resulted in the presumed TRPP2 dimer and trimer, but the same treatment of TRPP2_mut6 failed to produce these cross-linked adducts (Fig. 5*A*). (ii) While WT TRPP2 migrated as a trimer in BN-PAGE, TRPP2_mut6 migrated as a monomer (Fig. 5*B*).

Our experiments also showed that the interaction between full-length TRPP2 and PKD1 is abolished when the TRPP2 coiled coil domain trimer is disrupted. WT TRPP2 could be co-immunoprecipitated with PKD1 from HEK293T cells stably expressing FLAG-PKD1 and HA-TRPP2, with either an anti-HA or anti-FLAG antibody (Fig. 5*C*, lanes 1 and 3). In contrast, TRPP2_mut6 could not be co-immunoprecipitated with PKD1 from HEK293T

cells stably expressing FLAG-PKD1 and HA-TRPP2_mut6 (Fig. 5*C*, lanes 2 and 4). These results indicate that formation of the TRPP2 coiled coil domain trimer is necessary for full-length TRPP2 to form homotrimers and to form the TRPP2/PKD1 complex.

Disruption of the TRPP2 coiled coil domain trimer diminishes the surface expression of TRPP2 and PKD1. Previous studies indicate that the association of TRPP2 and PKD1 enhances the surface expression of both proteins (18, 20, 25). Abundant surface EGFP fluorescence spots were observed in oocytes expressing TRPP2-EGFP (Fig. S6*A*); however, few such spots were seen in oocytes expressing TRPP2_mut6-EGFP (Fig. S6*B*). Furthermore, while numerous TRPP2 fluorescence spots were observed on the plasma membrane when TRPP2 was coexpressed with PKD1 (Fig. 1*C*, Fig. 5*D* and Fig. S3*A*), very few TRPP2_mut6 fluorescence spots were detected when TRPP2_mut6 was coexpressed with PKD1 (Fig. 5*E*). These results indicate that both basal and PKD1-stimulated TRPP2 surface expression was abolished by the mut6 mutation. Conversely, few surface PKD1 fluorescence spots were observed in oocytes expressing PKD1-EGFP and TRPP2_mut6-mCherry (Fig. 5*E*), in contrast to the abundance of such spots in oocytes expressing PKD1-EGFP and TRPP2-mCherry (Fig. 1*F*, Fig. 5*D* and Fig. S3*A*), indicating that TRPP2-dependent PKD1 surface expression was also abolished by the mut6 mutation.

Discussion

Many proteins assemble or interact with their partners through coiled coil domains, which can associate homophilically and/or heterophilically to form dimers, trimers or tetramers (26-28). Our work shows that TRPP2 forms a homotrimer through a coiled coil domain (amino acids F839-A873) in the C terminus. This domain overlaps with the one (F839-D919) recently reported to be involved in homophilic TRPP2 interactions (29), but it differs from the one (E772-L796) previously postulated to play such a role (16). Our work further shows that a trimeric TRPP2 interacts with a single PKD1 to form a cell surface TRPP2/PKD1 complex, and that this 3:1 stoichiometric association is determined by an interaction between the newly identified TRPP2 coiled coil domain trimer and a previously identified (15) C terminal coiled coil domain of PKD1 (amino acids L4214 to R4248). The functional importance of these domains and their interactions is underscored by many naturally occurring ADPKD pathogenic mutations, including R4227X in PKD1 and R742X, R807X, E837X, and R872X in PKD2(2), which delete the coiled coil domains or the downstream “open“ region and, hence, abolish the assembly of the TRPP2/PKD1 complex.

It has been shown recently that a region in the C terminus of TRPM7 co-assembles to form an antiparallel four-stranded coiled coil (30). In contrast, our results demonstrate that the newly identified TRPP2 coiled coil domain assembles to form a trimer, both in solution (Fig. 2) and in crystal (Fig. 3 *C* and *F*). This coiled coil has many of the hallmarks of a canonical coiled coil (26-28),

in particular, the characteristic heptad repeat with hydrophobic residues at the 1st (i.e. *a*) and 4th (i.e. *d*) positions, and with charged residues at the 5th (i.e. *e*) and 7th (i.e. *g*) positions (Fig. 3*B*). Crystal structures show that this coiled coil domain forms a 3-stranded, parallel, bundle (Fig. 3 *C* and *F*), conforming to the propensity that opposite charges at the *e* and *g* positions (Fig. 3*B*) favor a parallel polarity of the α-helical chains (26-28). Interestingly, in the crystal lattice of the long fragment (i.e. TRPP2_G833-G895), the C terminal regions downstream of the coiled coil domain of one trimer interact with the same regions of another trimer (Fig. 3*E*). Even though this interaction appears to be an artifact caused by construct design and crystal packing, as alluded to above, the ability of this region to interact with other α-helices suggests that it might be the interacting site for the PKD1 coiled coil domain. This notion as well as the physical/chemical nature of the TRPP2/PKD1 interaction awaits further studies.

Although our results indicate that the newly identified TRPP2 coiled coil domain is necessary for the assembly of full-length homomeric TRPP2 complex, they do not exclude contributions from other regions. Indeed, an N terminal region was recently shown to be involved in TRPP2 oligomerization (31). Furthermore, disulfide bond(s) between TRPP2 subunits may also play a role, since full-length TRPP2 remains dimerized and trimerized under non-reducing but denaturing conditions (31) (Fig. 1*A*).

The 3:1 stoichiometry of the TRPP2/PKD1 complex is surprising, given that PKD1 has not generally been thought of as a channel-forming subunit (1, 4-

6, 11, 12, but see 32). If the channel pore of the TRPP2/PKD1 complex is formed by four subunits, the 3:1 stoichiometry would suggest either that PKD1 contributes to form the channel pore, in addition to its putative receptor functions, or that an endogenous oocyte protein, such as TRPC1 (23), associates with TRPP2 in a 1:3 stoichiometry to form the ion conduction pathway. These possibilities remain to be investigated. On first thought, PKD1 seems unlikely to be a channel-forming subunit since the original transmembrane topology prediction did not identify a pore-forming region (4). In that prediction, the region between the 10^{th} and 11^{th} transmembrane (TM) segments , which presumably correspond to the S5 and S6 TM segments of TRPP2, was only 7 amino acids long and was therefore too short to constitute a pore-forming loop. However, using 6 different contemporary programs for predicting TM segments, we find that the location of the last (i.e. 11^{th}) TM segment is uncertain. Four predictions place this TM segment ~25-36 amino acids away from the 10^{th} TM segment, long enough to form a pore loop. More intriguing, these 25-36 amino acids share ~50-55% similarity with the homologous putative pore-forming region in TRPP2. Thus, this region might constitute a pore-forming loop in PKD1.

TRPP2 forms spontaneously active non-selective cation channels in lipid bilayers (8, 9, 24). Functional expression of TRPP2 in *Xenopus* oocytes has also been reported (33). However, we failed to detect TRPP2-conducted currents when TRPP2 was expressed in oocytes (Fig. S7), even though plentiful TRPP2 proteins were detected on the plasma membrane (Fig. S6*A*). Also, in contrast to

previous observations in Chinese hamster ovary cells (18), we were unable to obtain spontaneously active currents that could be conclusively ascribed to TRPP2/PKD1 complexes in HEK 293T cells or *Xenopus* oocytes expressing TRPP2 and PKD1 (Fig. S7). This lack of current was not due to the lack of expression of the complexes on the surface membrane since both proteins were abundantly expressed (Fig. 1 *C* and *F*, Fig. 5D, and Fig. S3*A*). Finally, it has been reported that the TRPP2/PKD1 complex can be activated by an anti-PKD1 antibody raised against an epitope (E2939-N2956) in the extracellular N terminus in human PKD1 (20, 21). We produced two different batches of anti-mouse PKD1 serum raised against the corresponding region (E2931-N2948) in mouse PKD1. Both sera induced a current in HEK 293T cells or *Xenopus* oocytes expressing TRPP2 and PKD1; however, this current was also evoked by a control serum and was mostly likely conducted by channels unrelated to the TRPP2/PKD1 complex (Fig. S8). Thus, it remains a challenge to functionally characterize homomeric TRPP2 and heteromeric TRPP2/PKD1 complexes in these expression systems.

Several TRP channel subunits have been shown to form tetramers on their own (34-36). Single-channel recording and atomic force microscopy imaging suggest that homomeric TRPP2 complexes incorporated into lipid-bilayers are tetramers (24). Yet, our results indicate that TRPP2 predominantly forms a trimer when expressed in HEK 293 cells and oocytes, not only in the cell lysate (Fig. 1 *A and B*) but also in the plasma membrane (Fig. S3 *D and E*).

These results suggest that the association of the fourth subunit is significantly weaker than the trimeric assembly and that this association is potentially dynamic and regulated. A tightly bound TRPP2 trimer may associate with other channel-forming subunits, such as TRPC1(17, 21, 24) and TRPV4 (37), to form heterotetrameric channels, thereby greatly increasing its functional spectrum and versatility. It is of interest to note that the cyclic nucleotide-gated channels of rod photoreceptors also have a 3:1 stoichiometry, with 3 A1 and 1 B1 subunits (38-42), and that this stoichiometry is determined by a trimer-forming leucine-zipper domain in the C terminus of the A1 subunit (40).

Materials and Methods

Chemical cross-linking. Cell lysates were treated with freshly prepared disuccinimidyl tartarate (DST, Pierce) on ice for 4 hrs.

Total Internal Reflection Microscopy (TIRF) and determination of bleaching steps. *Xenopus* oocytes were enzymatically treated to enable close contact to the coverslip (22). Movies were acquired with a back-illuminated EMCCD camera (Andor iXon DV-897 BV). Gaussian profile was fitted to the raw images to determine the time course of the emission intensity. Fluorescent spots that stayed immobile were selected, and bleaching steps were counted manually.

Light scattering. Purified Proteins were run through a gel filtration column and the eluates were examined by static light scattering (Wyatt Technology).

Crystallization, data collection and Structure determination. Crystallization was carried out by using the hanging-drop vapour diffusion method at 20 °C. Crystals were rinsed in Paratone-N (Hampton Research), and flash-frozen in liquid nitrogen for data collection at 100 K. Molecular replacement method was used to determine the structures. Data collection and refinement statistics are summarized in Table S1.

Other materials and methods. Details for the methods described above and for construct cloning, cell culture, transfection and stable line generation, SDS-PAGE, BN-PAGE and Western blot, protein fragment expression and purification, coimmunoprecipitation, anti-PKD1 serum generation, and electrophysiology are provided in SI *Materials and Methods*.

ACKNOWLEDGMENTS

We thank Dr. Yiqiang Cai at Yale University for human TRPP2 cDNA and Dr. Hiroaki Matsunami at Duke University for HEK 293T cells. We also thank Dr. Farhad Forouhar at Columbia University for suggestions on structural determination, and Dr. Ioannis Michailidis at Columbia University for reading the manuscript. This work was supported by NIH grants NS045383 and GM085234 (to J.Y.) and NS035549 (to E.Y.I.), NIH grants to L.T., the Established Investigator Award from the American Heart Association (to J.Y.), a Postdoctoral Fellowship from the American Heart Association (to M.H.U.), Canadian Institutes of Health Research grants (to X.-Z.C.), and a Wellcome Trust Research Leave Award (to A.C.M.O.).

Reference

1. Ong AC & Harris PC (2005) Molecular pathogenesis of ADPKD: the polycystin complex gets complex. *Kidney Int* 67:1234-1247.
2. Wu G & Somlo S (2000) Molecular genetics and mechanism of autosomal dominant polycystic kidney disease. *Mol Genet Metab* 69:1-15.
3. Harris PC & Torres VE (2009) Polycystic Kidney Disease. *Annu Rev Med* 60:321–337.
4. Hughes J*, et al.* (1995) The polycystic kidney disease 1 (PKD1) gene encodes a novel protein with multiple cell recognition domains. *Nat Genet* 10:151-160.
5. Giamarchi A*, et al.* (2006) The versatile nature of the calcium-permeable cation channel TRPP2. *EMBO Rep* 7:787-793.
6. Delmas P (2005) Polycystins: polymodal receptor/ion-channel cellular sensors. *Pflugers Arch* 451:264-276.
7. Mochizuki T*, et al.* (1996) PKD2, a gene for polycystic kidney disease that encodes an integral membrane protein. *Science* 272:1339-1342.
8. Gonzalez-Perrett S*, et al.* (2001) Polycystin-2, the protein mutated in autosomal dominant polycystic kidney disease (ADPKD), is a Ca^{2+}-permeable nonselective cation channel. *Proc Natl Acad Sci U S A* 98:1182-1187.
9. Koulen P*, et al.* (2002) Polycystin-2 is an intracellular calcium release channel. *Nat Cell Biol* 4:191-197.
10. Luo Y, Vassilev PM, Li X, Kawanabe Y, & Zhou J (2003) Native polycystin 2 functions as a plasma membrane Ca^{2+}-permeable cation channel in renal epithelia. *Mol Cell Biol* 23:2600-2607.
11. Kottgen M (2007) TRPP2 and autosomal dominant polycystic kidney disease. *Biochim Biophys Acta* 1772:836-850.
12. Tsiokas L, Kim S, & Ong EC (2007) Cell biology of polycystin-2. *Cell Signal* 19:444-453.
13. Kottgen M & Walz G (2005) Subcellular localization and trafficking of polycystins. *Pflugers Arch* 451:286-293.
14. Nauli SM*, et al.* (2003) Polycystins 1 and 2 mediate mechanosensation in the primary cilium of kidney cells. *Nat Genet* 33:129-137.
15. Qian F*, et al.* (1997) PKD1 interacts with PKD2 through a probable coiled-coil domain. *Nat Genet* 16:179-183.
16. Tsiokas L, Kim E, Arnould T, Sukhatme VP, & Walz G (1997) Homo- and heterodimeric interactions between the gene products of PKD1 and PKD2. *Proc Natl Acad Sci U S A* 94:6965-6970.
17. Tsiokas L*, et al.* (1999) Specific association of the gene product of PKD2 with the TRPC1 channel. *Proc Natl Acad Sci U S A* 96:3934-3939.
18. Hanaoka K*, et al.* (2000) Co-assembly of polycystin-1 and -2 produces unique cation-permeable currents. *Nature* 408:990-994.

19. Newby LJ*, et al.* (2002) Identification, characterization, and localization of a novel kidney polycystin-1-polycystin-2 complex. *J Biol Chem* 277:20763-20773.
20. Delmas P*, et al.* (2004) Gating of the polycystin ion channel signaling complex in neurons and kidney cells. *Faseb J* 18:740-742.
21. Bai CX*, et al.* (2008) Formation of a new receptor-operated channel by heteromeric assembly of TRPP2 and TRPC1 subunits. *EMBO Rep* 9:472-479.
22. Ulbrich MH & Isacoff EY (2007) Subunit counting in membrane-bound proteins. *Nat Methods* 4:319-321.
23. Maroto R*, et al.* (2005) TRPC1 forms the stretch-activated cation channel in vertebrate cells. *Nat Cell Biol* 7:179-185.
24. Zhang P*, et al.* (2009) The multimeric structure of polycystin-2 (TRPP2): structural-functional correlates of homo- and hetero-multimers with TRPC1. *Hum Mol Genet* 18:1238-1251.
25. Grimm DH*, et al.* (2003) Polycystin-1 distribution is modulated by polycystin-2 expression in mammalian cells. *J Biol Chem* 278:36786-36793.
26. Lupas AN & Gruber M (2005) The structure of alpha-helical coiled coils. *Adv Protein Chem* 70:37-78.
27. Parry DA, Fraser RD, & Squire JM (2008) Fifty years of coiled-coils and alpha-helical bundles: a close relationship between sequence and structure. *J Struct Biol* 163:258-269.
28. Woolfson DN (2005) The design of coiled-coil structures and assemblies. *Adv Protein Chem* 70:79-112.
29. Celic A, Petri ET, Demeler B, Ehrlich BE, & Boggon TJ (2008) Domain mapping of the polycystin-2 C-terminal tail using de novo molecular modeling and biophysical analysis. *J Biol Chem* 283:28305-28312.
30. Fujiwara Y & Minor DL, Jr. (2008) X-ray crystal structure of a TRPM assembly domain reveals an antiparallel four-stranded coiled-coil. *J Mol Biol* 383:854-870.
31. Feng S*, et al.* (2008) Identification and functional characterization of an N-terminal oligomerization domain for polycystin-2. *J Biol Chem* 283:28471-28479.
32. Babich V*, et al.* (2004) The N-terminal extracellular domain is required for polycystin-1-dependent channel activity. *J Biol Chem* 279:25582-25589.
33. Vassilev PM*, et al.* (2001) Polycystin-2 is a novel cation channel implicated in defective intracellular Ca(2+) homeostasis in polycystic kidney disease. *Biochem Biophys Res Commun* 282:341-350.
34. Cheng W, Yang F, Takanishi CL, & Zheng J (2007) Thermosensitive TRPV channel subunits coassemble into heteromeric channels with intermediate conductance and gating properties. *J Gen Physiol* 129:191-207.

35. Hoenderop JG*, et al.* (2003) Homo- and heterotetrameric architecture of the epithelial Ca^{2+} channels TRPV5 and TRPV6. *The EMBO journal* 22:776-785.
36. Mio K*, et al.* (2007) The TRPC3 channel has a large internal chamber surrounded by signal sensing antennas. *J Mol Biol* 367:373-383.
37. Kottgen M*, et al.* (2008) TRPP2 and TRPV4 form a polymodal sensory channel complex. *The Journal of cell biology* 182:437-447.
38. Weitz D, Ficek N, Kremmer E, Bauer PJ, & Kaupp UB (2002) Subunit stoichiometry of the CNG channel of rod photoreceptors. *Neuron* 36:881-889.
39. Zheng J, Trudeau MC, & Zagotta WN (2002) Rod cyclic nucleotide-gated channels have a stoichiometry of three CNGA1 subunits and one CNGB1 subunit. *Neuron* 36:891-896.
40. Zhong H, Lai J, & Yau KW (2003) Selective heteromeric assembly of cyclic nucleotide-gated channels. *Proc Natl Acad Sci U S A* 100:5509-5513.
41. Zhong H, Molday LL, Molday RS, & Yau KW (2002) The heteromeric cyclic nucleotide-gated channel adopts a 3A:1B stoichiometry. *Nature* 420:193-198.
42. Matulef K & Zagotta WN (2003) Cyclic nucleotide-gated ion channels. *Annu Rev Cell Dev Biol* 19:23-44.

Figure Legends

Fig. 1. Subunit stoichiometry of full length homomeric TRPP2 and heteromeric TRPP2/PKD1 complexes. (*A*) Western blot following BN-PAGE of purified HA-TRPP2. In lanes 2 and 3, the sample was incubated at 70 ^{o}C for 10 min with 2% SDS plus 100 mM DTT or with 2% SDS. TRPP2 was detected with an anti-HA antibody, and putative TRPP2 monomer, dimer and trimer are indicated. (*B*) Western blot following SDS-PAGE showing the cross-linking products of TRPP2. Cross-linking was carried out with 1 mM DST. The putative subunit composition of the bands is indicated. (*C and F*) TIRF image of EGFP and mCherry fluorescence from an oocyte expressing the indicated constructs, showing spots that exhibited EGFP and mCherry dual fluorescence and were immobile (circles). Other spots do not fit analysis criteria. Scale bar, 2 μm. (*D*) Time course of photobleaching of two representative PKD1-mCherry and TRPP2-EGFP dual-fluorescence spots, showing three EGFP bleaching steps (arrows). mCherry and EGFP excitation is indicated by red and green bar, respectively. (*E*) Distribution of observed EGFP bleaching steps (green bars) for PKD1-mCherry and TRPP2-EGFP dual-fluorescence spots compared to calculated distribution based on 83% of EGFPs being fluorescent (white bars). No events with 5 or more bleaching steps were observed. (*G*) Time course of photobleaching of two representative PKD1-EGFP and TRPP2-mCherry dual-fluorescence spots showing one EGFP

bleaching step (arrow). (*H*) Distribution of EGFP bleaching steps for PKD1-EGFP and TRPP2-mCherry dual-fluorescence spots.

Fig. 2. The complex formed by TRPP2 and PKD1 C terminal interacting domains has 3 TRPP2 and 1 PKD1. Bar graph compares the calculated and measured M.W. (determined by static light scattering) of the indicated proteins. The calculated M.W. was obtained according to the stoichiometry schematized on the right. The protein fragments (indicated at the bottom) were tagged with either hexahistidine (His_6), MBP or His_6 plus SUMO. MBP and SUMO also served to increase the resolution and accuracy of the M.W. measurement. MBP-His_6 was used as a control to demonstrate the accuracy of the equipment. Results are shown as mean and s.d. n=number of measurements.

Fig. 3. Crystal structures of the TRPP2 coiled coil domain reveal that it forms a trimer. (*A*) Amino acid sequence alignment of a TRPP2 C terminal fragment (G833-G895 in human) from the indicated species. NCBI accession numbers for sequences used here: EAX06011 (human), NP_032887(mouse), NP_001026311(chicken), NP_001002310(zebrafish), and NP_999827(sea urchin). *Strongylocentrotus purpuratus. Red: residues identical to those in human. Green: similar residues. Blue bar indicates a predicted coiled coil domain; green bar indicates the “open” region seen in the crystal structure in (*C*). (*B*) Heptad repeats of the predicted coiled coil domain in (*A*). Residue number is

given on both sides of the sequence. Letters *a*-*g* designate the position of the amino acids within the heptad. Positions *a* and *d* are invariantly hydrophobic, a characteristic of coiled coil domains. (*C*) Crystal structure of TRPP2_G833-G895. G833-R872 is colored blue and A873-G895 green. (*D*) Side-chain of amino acids involved in the trimeric coiled coil interactions. For clarity, one subunit is removed. Residues in red were mutated to alanine to generate "mut6". (*E*) Packing of TRPP2_G833-G895 trimers in crystal. Two trimers interact with each other through their C termini to form a hexamer, as exemplified by the pair colored in blue and orange. The unit cell is defined by the purple box. (*F*) Crystal structure of TRPP2_G833-R872. Residues V834-M870 were resolved in the structure. (*G*) Superposition of the structures of TRPP2_G833-G895 and TRPP2_G833-R872.

Fig. 4. The TRPP2 trimer is essential for the formation of the TPPP2/PKD1 coiled coil domain complex. (*A*) SDS-PAGE showing the interaction or the lack thereof between the indicated PKD1 and TRPP2 fragments (schematized in the lower right corner). The MBP-tagged PKD1 fragment was used to pull down the indicated SUMO-tagged TRPP2 fragments (upper gel), which showed similar level of expression (lower gel, arrows indicated the corresponding protein bands). (*B*) Gel filtration profile of MBP-tagged WT TRPP2_G821-S926 and TRPP2_G821-S926_mut6 (schematized on top, with stars denoting the mut6 mutation). The right shift of the latter indicates a M.W. decrease, as confirmed

by static light scattering measurements (M.W. shown in graph). (*C*) SDS-PAGE showing that mut6 abolishes interaction between the indicated PKD1 and TRPP2 fragments. The MBP-tagged PKD1 fragment was used to pull down the indicated SUMO-tagged TRPP2 fragments (upper gel), which showed a similar level of expression (lower gel).

Fig. 5. The TRPP2 coiled coil domain trimer is essential for the formation of TRPP2 homomeric and TRPP2/PKD1 heteromeric complexes. (*A*) Western blot following SDS-PAGE showing the lack of cross-linking of TRPP2_mut6 subunits. Cross-linking reaction (with the indicated concentration of DST) was carried out in the lysate of HEK 293T cells stably expressing either HA-TRPP2 or HA-TRPP2_mut6. Here, and in *B* and *C*, TRPP2 was detected with an anti-HA antibody. Putative TRPP2 monomer, dimer and trimer are indicated. (*B*) Western blot following BN-PAGE of purified HA-TRPP2 (WT) or HA-TRPP2_mut6 (mut6). Putative TRPP2 monomer and trimer are indicated. (*C*) Western blot following SDS-PAGE showing that WT TRPP2 but not TRPP2_mut6 can be co-immunoprecipitated with PKD1. Immunoprecipitation (IP) was carried out with either an anti-HA or an anti-FLAG antibody using the lysates of HEK 293T cells stably expressing either FLAG-PKD1 and HA-TRPP2 (lanes 1 and 3) or FLAG-PKD1 and HA-TRPP2_mut6 (lanes 2 and 4). (*D* and *E*) TIRF image of EGFP and mCherry fluorescence from an oocyte expressing the indicated combinations of constructs. Scale bar, 2 μm.

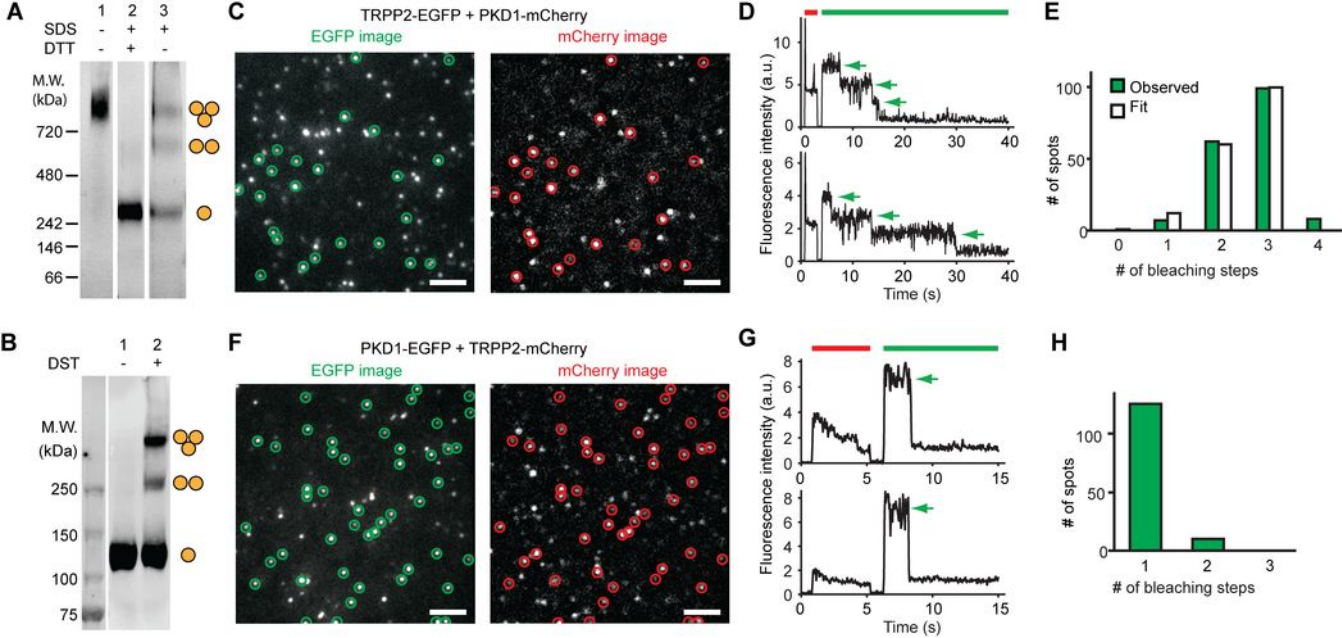
A
1 2 3
SDS - + +
DTT - + -
M.W. (kDa)
720
480
242
146
66
B
1 2
DST - +
M.W. (kDa)
250
150
100
75
C
TRPP2-EGFP + PKD1-mCherry
EGFP image
mCherry image
D
Fluorescence intensity (a.u.)
Time (s)
E
Observed
Fit
# of spots
# of bleaching steps
F
PKD1-EGFP + TRPP2-mCherry
EGFP image
mCherry image
G
Fluorescence intensity (a.u.)
Time (s)
H
# of spots
# of bleaching steps

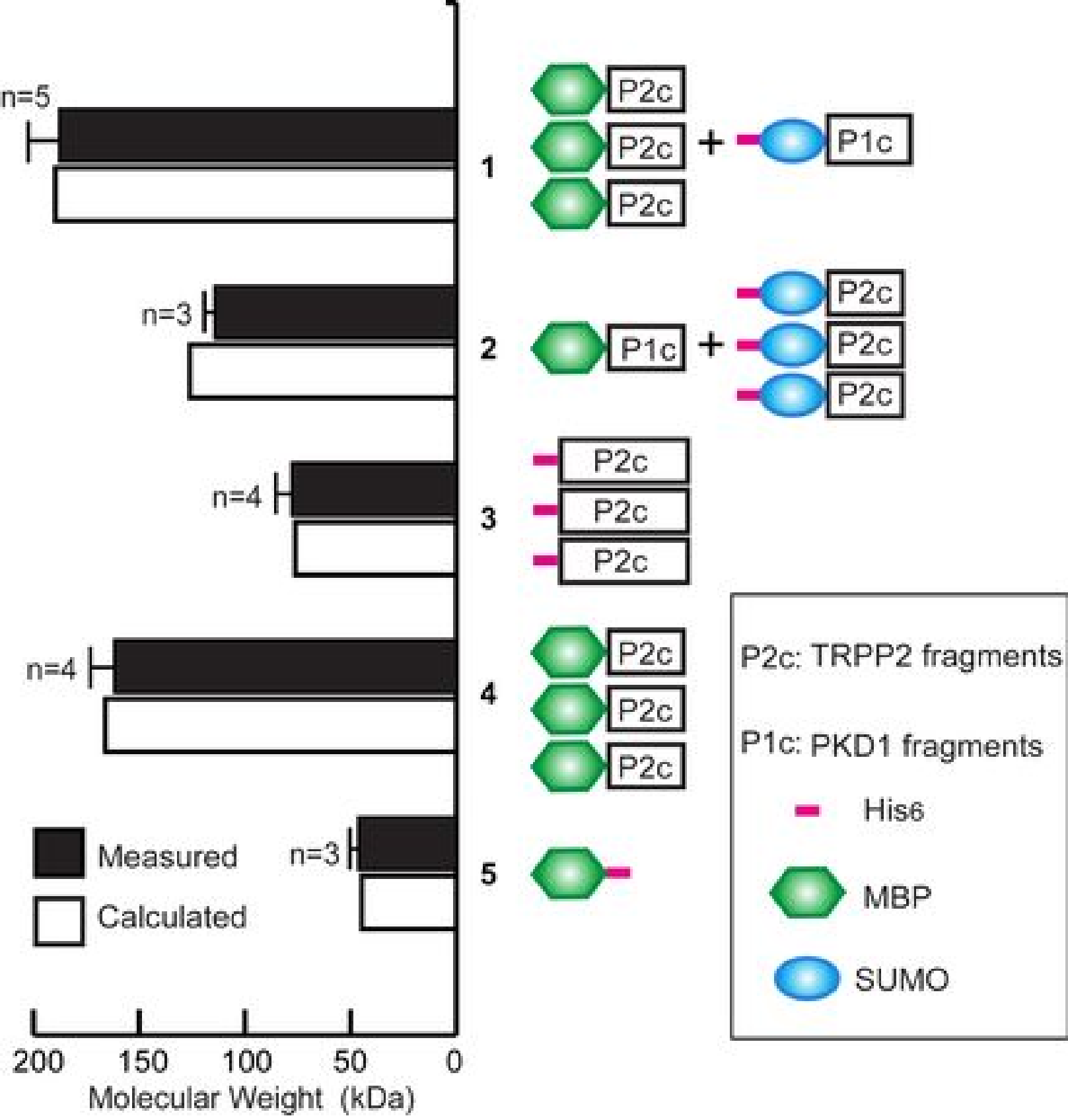

1: MBP-TRPP2_G821-S926 + SUMO-PKD1_S4191-G4279
2: MBP-PKD1_S4191-G4279 + SUMO-TRPP2_G833-S918
3: His6-TRPP2_D723-G928
4: MBP-TRPP2_G821-S926
5: MBP-His6

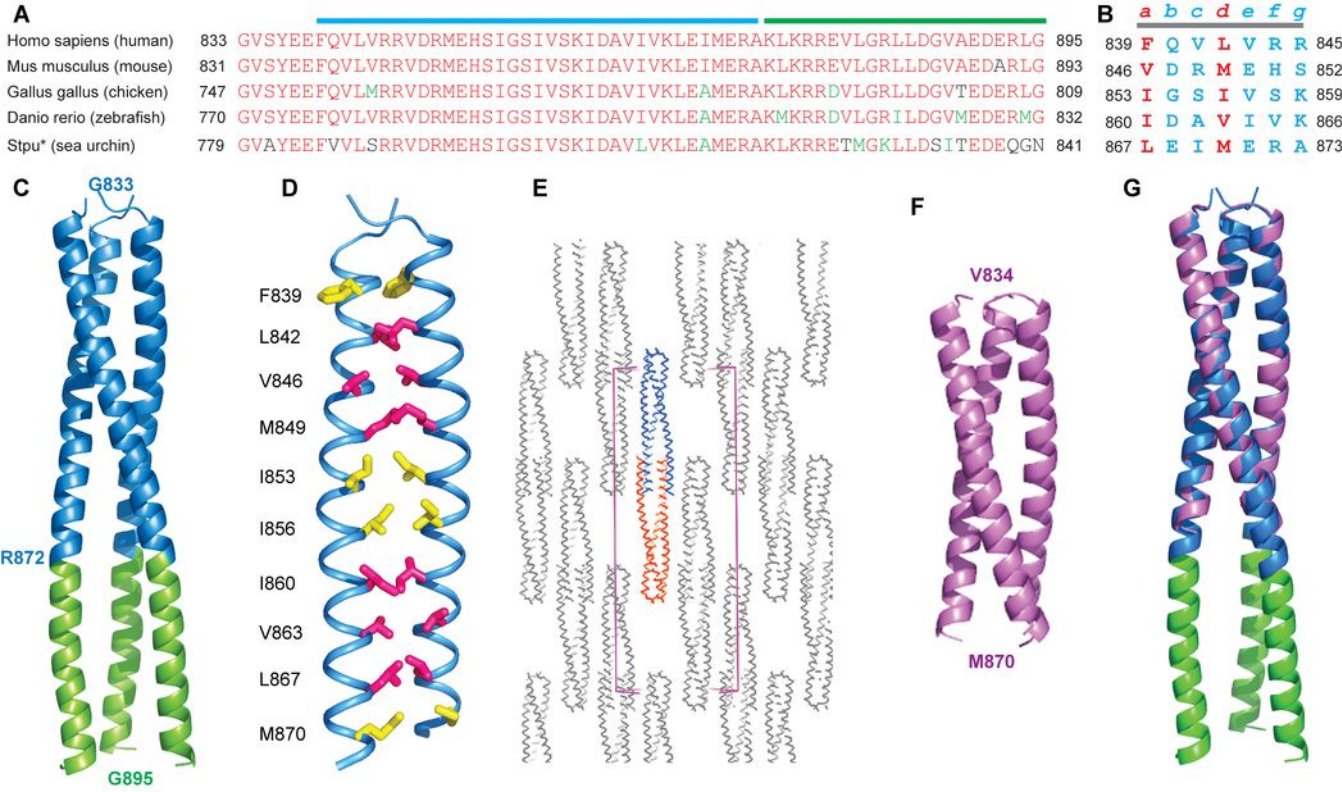
A
Homo sapiens (human) 833 GVSYEEFQVLVRRVDRMEHSIGSIVSKIDAVIVKLEIMERAKLKRREVLGRLLDGVAEDERLG 895
Mus musculus (mouse) 831 GVSYEEFQVLVRRVDRMEHSIGSIVSKIDAVIVKLEIMERAKLKRREVLGRLLDGVAEDARLG 893
Gallus gallus (chicken) 747 GVSYEEFQVLMRRVDRMEHSIGSIVSKIDAVIVKLEAMERAKLKRRDVLGRLLDGVTEDERLG 809
Danio rerio (zebrafish) 770 GVSYEEFQVLVRRVDRMEHSIGSIVSKIDAVIVKLEAMERAKMKRRDVLGRILDGVMEDERMG 832
Stpu* (sea urchin) 779 GVAYEEFVVLSRRVDRMEHSIGSIVSKIDAVLVKLEAMERAKLKRRETMGKLLDSITEDEQGN 841
B
a b c d e f g
839 F Q V L V R R 845
846 V D R M E H S 852
853 I G S I V S K 859
860 I D A V I V K 866
867 L E I M E R A 873
C
G833
R872
G895
D
F839
L842
V846
M849
I853
I856
I860
V863
L867
M870
E
F
V834
M870
G

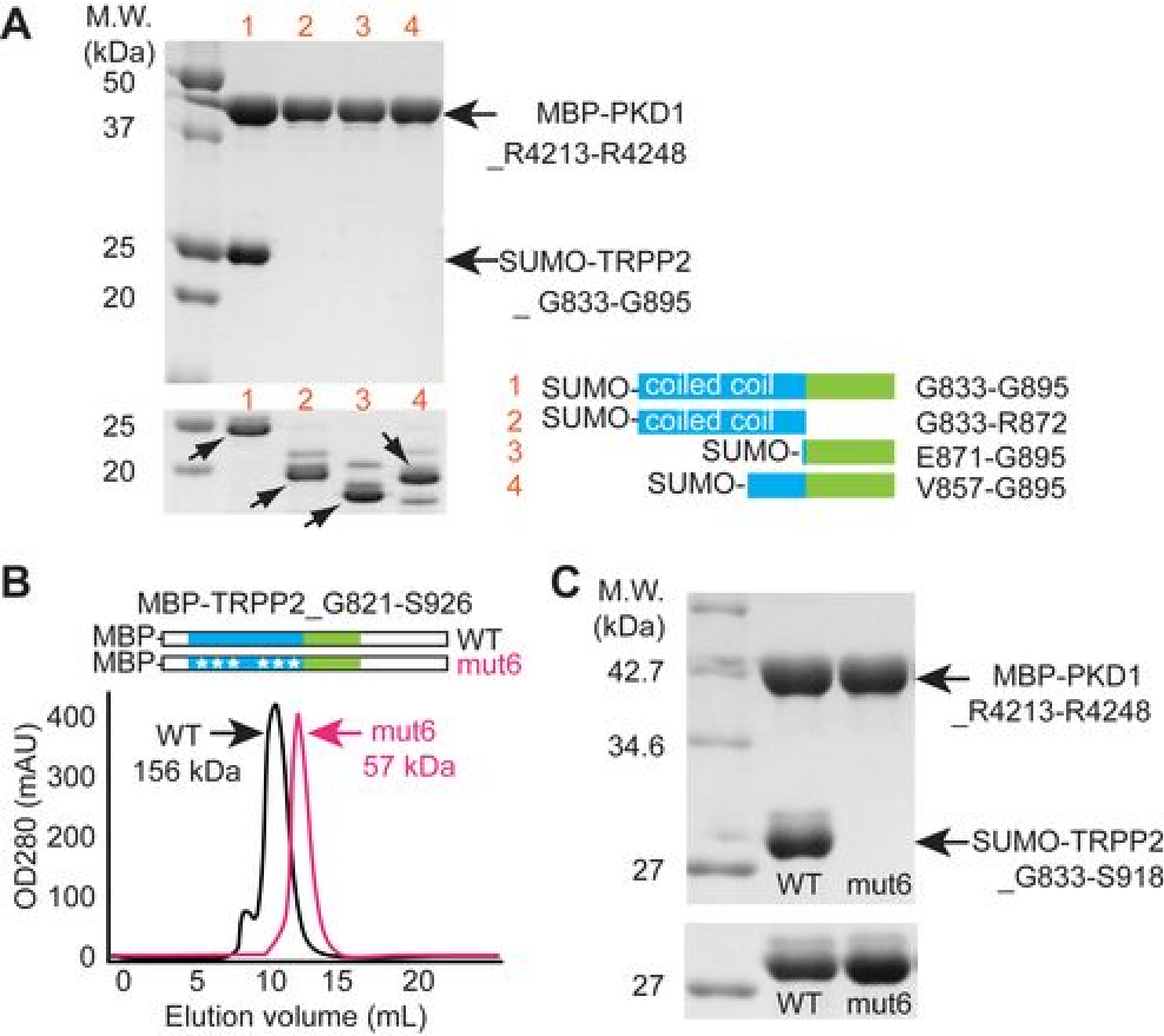
A
M.W.
(kDa)
50
37
25
20
1 2 3 4
MBP-PKD1
_R4213-R4248
SUMO-TRPP2
_ G833-G895
1 SUMO- coiled coil G833-G895
2 SUMO- coiled coil G833-R872
3 SUMO- E871-G895
4 SUMO- V857-G895
B
MBP-TRPP2_G821-S926
MBP
WT
MBP
mut6
OD280 (mAU)
400
300
200
100
0
WT
156 kDa
mut6
57 kDa
0 5 10 15 20
Elution volume (mL)
C
M.W.
(kDa)
42.7
34.6
27
MBP-PKD1
_R4213-R4248
SUMO-TRPP2
_G833-S918
WT mut6
27
WT mut6

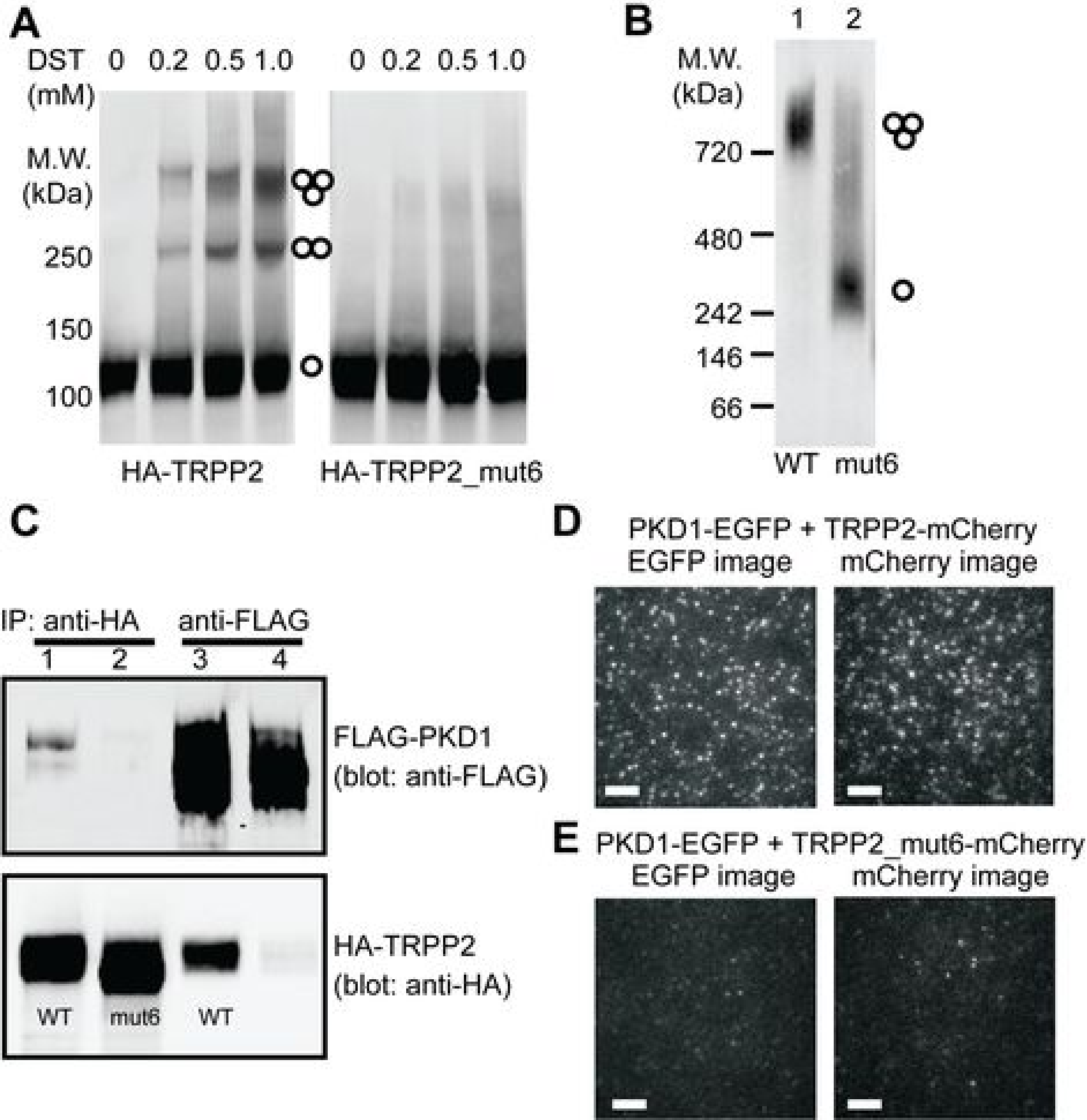
A
DST (mM)
0 0.2 0.5 1.0
0 0.2 0.5 1.0
M.W. (kDa)
250
150
100
HA-TRPP2
HA-TRPP2_mut6
B
1 2
M.W. (kDa)
720
480
242
146
66
WT mut6
C
IP: anti-HA
anti-FLAG
1 2 3 4
FLAG-PKD1
(blot: anti-FLAG)
HA-TRPP2
(blot: anti-HA)
WT mut6 WT
D
PKD1-EGFP + TRPP2-mCherry
EGFP image
mCherry image
E
PKD1-EGFP + TRPP2_mut6-mCherry
EGFP image
mCherry image

Supplementary Information for:

Structural and molecular basis of the assembly of the TRPP2/PKD1 complex

Yong Yu[a], Maximilian H. Ulbrich[b], Ming-hui Li[a], Zafir Buraei[a], Xing-Zhen Chen[d], Albert C.M. Ong[e], Liang Tong[a], Ehud Y. Isacoff[b,c] and Jian Yang[a, 1]

[a]Department of Biological Sciences, Columbia University, New York, NY 10027, USA

[b]Department of Molecular and Cell Biology, University of California, Berkeley, CA 94720, USA

[c]Material Sciences & Physics Biosciences Divisions, Lawrence Berkeley National Laboratory, Berkeley, CA 94720, USA

[d]Membrane Protein Research Group, Department of Physiology, Faculty of Medicine and Dentistry, University of Alberta, Edmonton, Alberta, T6G 2H7, Canada

[e]Kidney Genetics Group, Academic Unit of Nephrology, Sheffield Kidney Institute, School of Medicine and Biomedical Sciences, University of Sheffield, Sheffield, UK

[1] To whom correspondence should be addressed.

Jian Yang, Department of Biological Sciences, 917 Fairchild Center, MC2462, Columbia University, New York, NY 10027

Phone: (212)-854-6161; Fax: (212)-531-0425 Email: jy160@columbia.edu

SI Materials and Methods

Constructs and cloning. For constructs used to generate stable cell lines for chemical cross-linking, blue native PAGE and co-immunoprecipitation experiments, a HA (human influenza hemagglutinin) tag was added to the N terminus of wild type or mutant full-length human TRPP2 cDNA (gift of Dr. Yiqiang Cai at Yale University, NCBI accession number U50928), and the whole construct was cloned into the pIREShyg3 vector (Clontech); also, the signal peptide (the first 23 amino acids in the N terminus) of mouse PKD1 (NCBI accession number NM_013630) was replaced by a Ig k-chain leader sequence (from the pDisplay vector from Invitrogen) and a FLAG tag was added immediately after this sequence, and this construct was cloned into the pIRESpuro2 vector (Clontech).

For constructs used in single-molecule photobleaching experiments, a modified pGEMHE vector was generated by inserting the EGFP or mCherry cDNA at the multiple cloning sites. The GFP variant used was monomeric EGFP (EGFP from Clontech's pEGFP-N1 with an A206K mutation). mCherry was a gift from Roger Tsien at the University of California, San Diego (1). Wild type or mutant human TRPP2 or mouse PKD1 cDNA was inserted before EGFP or mCherry to generate fusion proteins with a flexible linker (SRGTSGGSGGSRGSGGSGG) in between. Thus, the final constructs are mouse PKD1 (or TRPP2)–19 amino acid-linker–EGFP (or mCherry).

Although only TRPP2_G833-G895 was found in the protein crystal, we actually set up crystallization of a protein complex of this fragment and a human PKD1 fragment (PKD1_G4204-R4252, NCBI accession number L39891). To make this complex, cDNA encoding amino acids G833-G895 of human TRPP2 was cloned into the second multiple cloning site of the pETDuet-1 vector (Novagen) with restriction enzymes Nde I and XhoI. As a result, an extra methionine was introduced at the N terminus of the TRPP2 peptide. The cDNAs for PKD1_G4204-R4252, and another shorter TRPP2 construct TRPP2_G833-R872, which was used for crystallization by itself, were cloned into the pET-28a(+) vector (Novagen) with restriction enzymes Nde I and Xho I. As a result, a stretch of 22 amino acids (MGSSHHHHHHSSGLVPRGSHM) containing a His_6 tag and a thrombin cleavage site was introduced at the N terminus of the expressed peptides.

For constructs used in pull-down and light scattering experiments, PCR-generated human TRPP2 and human PKD1 fragments were cloned into either pMAL-c2x (New England Biolabs) or a modified pET-28a(+) vector, which has an inserted yeast Small Ubiquitin-like Modifier (SUMO) cDNA, thus producing maltose binding protein (MBP) or SUMO tagged proteins. The C-terminal hexahistidine (His_6)-tagged MBP construct used in light scattering experiments was generated by cloning MBP cDNA into the pET-26b(+) vector (Novagen). The His_6-tagged TRPP2 construct was cloned into the pET-28a(+) vector.

Cell culture, transfection and generation of stable cell lines. HEK293T cells (gift of Dr. Hiroaki Matsunami at Duke University) were maintained in a DMEM medium containing 10% FBS, 50 U/ml penicillin and 50 μg/ml streptomycin. Lipofectamine 2000 (Invitrogen) was used for all transfections. To generate cell lines stably expressing HA-TRPP2,HA-TRPP2_mut6 or FLA-PKD1, cell culture media were changed to selective media with 200 μg/ml Hygromycin B (Invitrogen) or 2 μg/ml puromycin (sigma) 36 hrs after transfection. Cells were cultured in selective media for ~2 weeks and positive clones were picked and tested with immunofluorescence using a mouse monoclonal anti-HA antibody HA.11 (Covance) or a mouse monoclonal anti-FLAG antibody M2 (Sigma). Those cell lines that gave excellent immunofluorescence signals were further tested by Western blot. To verify the expression of full-length TRPP2, HA-TRPP2-expressing lines were tested in Western blots with the HA.11 anti-HA antibody and another mouse monoclonal anti-TRPP2 antibody 1A11, which recognizes the C terminus of TRPP2 (2). FLAG-PKD1-expressing lines were tested in Western-blots with the M2 anti-FLAG antibody. Cells stably expressing both HA-TRPP2 (or HA-TRPP2_mut6) and FLAG-PKD1 were generated by transfecting FLAG-PKD1 (in pIRESpuro2) into HA-TRPP2 or HA-TRPP2_mut6 stable lines, followed by selection with 2 ug/ml puromycin (Sigma). These lines were first screened with immunofluorescence using the M2 anti-FLAG antibody. The expression of full-length FLAG-PKD1 was verified by Western blots with the M2 anti-FLAG antibody and another mouse monoclonal anti-PKD1 antibody, 7e12, which recognizes the leucine-rich repeat in the N terminus (3).

SDS-PAGE, blue native PAGE and Western blot. SDS-PAGE was performed in Tris-glycine buffer under reducing condition with 15% acrylamide gel for pull-down experiments and 4-15% linear gradient Tris-HCl gel (Bio-Rad) for cross-linking and co-immunoprecipitation experiments. Precision Plus Protein All Blue Standards (Bio-Rad) or broad range protein M.W. standards (Invitrogen) was used as M.W. markers. The M.W. of the protein samples was estimated from its retardation factor (R_f) on a plot of the R_f values of the protein markers versus the log of their M.W.

Blue native PAGE (BN-PAGE) (4) was performed with the NativePAGE Novex Bis-Tris Gel System (Invitrogen), and 3-12% gels were used by following the manufacturer's protocol. Samples were purified with beads that are coated with an anti-HA antibody (Covance) as in co-immunoprecipitation experiments, except that the proteins were eluted from the beads with a solution containing 1X NativePAGE sample buffer (Invitrogen), 0.4 mg/ml HA peptide (GenScript), 1% DDM, and 1/50 (V/V) protease inhibitor cocktail (Sigma). Elution was carried out at 4 °C for 15 min. 0.25% Coomassie blue G-250 was added into the samples immediately prior to electrophoresis. Denatured or both denatured and reduced samples were obtained by adding either 2% SDS (w/v) alone or 2% SDS and 100 mM DTT to the solution and incubating the sample at 70 °C for 10 min. NativeMark unstained protein standard (Invitrogen) was used for BN-PAGE, and markers' positions were identified by staining the transferred PVDF membrane with Ponceau S (Sigma) before performing the Western blot.

Western blot: after electrophoresis, the protein gel was transferred to the PVDF membrane and processed with the One-step fluorescence Western-blot kit (GenScript). The monoclonal mouse anti-HA antibody HA.11 (Covance) or the monoclonal mouse anti-PKD1 antibody 7e12 was used as the primary antibody. Alexa Fluor 680 goat anti-mouse IgG (Invitrogen) was used as the secondary antibody in cross-linking and co- immunoprecipitation experiments, and IRDye 800CW goat anti-mouse IgG (Li-COR) was used in BN-PAGE experiments. Images were scanned and analyzed with the Odyssey Infrared Imaging System (Li-COR).

Chemical cross-linking. Stable cell lines expressing the desired constructs were washed twice with cold PBS solution, then harvested and resuspended in a lysis solution containing 1 X phosphate-buffered saline (PBS), pH 7.4, 2.5 % n-Dodecyl β-D-maltoside (DDM), 1 mM EDTA, 10% glycerol and 1/50 (V/V) Protease Inhibitor Cocktail (sigma). After rotating at 4 °C for 1 hr, samples were centrifuged at 16,000 g for 30 min, and cell lysate was collected from the supernatant. Fresh cross-linker stock solutions were prepared by dissolving disuccinimidyl tartarate (DST, Pierce) into DMSO. Cross-linking reactions were carried out by diluting the stock solution into the cell lysate samples, followed by incubation on ice for 4 hrs. SDS sample buffer was subsequently added to stop the reaction. The samples were then incubated at 37 °C for 30 min, and the cross-linking products were analyzed by SDS-PAGE and Western blot.

Total Internal Reflection Microscopy. cDNAs were linearized with an appropriate restriction enzyme after the polyadenylation sequence and transcribed *in vitro* using the T7 polymerase. cRNAs were injected into *Xenopus laevis* oocytes. The amounts of cRNA injected per oocyte were 10ng for PKD1 and 5ng for TRPP2 constructs, dissolved in 50nl H_2O. 12-48 hrs after cRNA injection and expression at 18 ºC, the oocytes were enzymatically treated with 1mg/ml hyaluronidase (Sigma) and 1U/ml neuraminidase (Sigma) for 15min at 4 °C and manually devitellinized to enable close contact of the oocyte's plasma membrane to the coverslip (5, 6). The coverslips' refractive index (n=1.78) matched the refractive index of the microscope objective front lens (Olympus 100x/NA1.65) and the immersion oil (Cargille). Movies of 500-800 frames of a 13X13 μm^2 area were acquired at frame rates of 30Hz with a back-illuminated EMCCD camera (Andor iXon DV-897 BV) after an additional 3x magnification. EGFP was excited with a 488 nm Argon laser, and mCherry with a 593 nm DPSS laser. Laser powers were between 0.5 mW and 2 mW, and the diameter of the beam at the sample was about 20µm. For imaging of EGFP and mCherry from the same sample, we used a double dichroic mirror (z488-594rpc, Chroma) and switched between emission filters (525/50 for EGFP, 629/53 for mCherry, Semrock) using electromechanical shutters and a motorized filter wheel. First, fluorescence from mCherry was measured, and after complete bleaching of mCherry, EGFP fluorescence was measured. The time for switching off the 593 nm illumination, changing emission filter, and switching on the 488 nm illumination was 1 to 2 s.

Extraction of spot positions and number of bleaching steps. In order to determine the positions of the fluorescent proteins, the first few frames for each color were extracted from the movies and averaged. The number of frames for averaging was based on the bleaching time of the fluorophore and varied between 3 and 10 frames. A spatial high-pass filter with a filter constant of 15 pixels (750 nm) for removal of background fluorescence and a low-pass filter with a filter constant of 1.5 pixels (75 nm) for reduction of noise were applied. Peaks down to an appropriate intensity threshold were selected, and Gaussian profiles were fitted to the spots for exact determination of the center position. The spot positions from the red and the green channel were overlaid, and spots closer than 3 pixels (150 nm) were considered to be co-localized. To determine the time course of the emission intensity from a fluorescent spot, a Gaussian profile with a full width at half maximum of 6 pixels (300 nm) around the previously determined center position was fitted to the raw images. We selected fluorescent spots that stayed immobile during the movie (~40%), discarded traces that showed emission intensities with no clear bleaching steps, and manually counted the number of bleaching steps from the remaining spots.

Protein fragments expression and purification. To purify the TRPP2_G833-G895/ His_6-PKD1_G4204-R4252 complex used for crystallization, pETDuet-1 containing TRPP2_G833-G895 and pET-28a(+) containing PKD1_G4204-R4252 were co-transformed into Rosetta 2(DE3) cells (Novagen). Bacteria were grown

at 37 °C until OD_{600} reached 0.6. The cultures were then cooled down to 24 °C and 1 mM IPTG was added to induce protein expression. After 5 hrs of induction, bacteria were collected at 4000 rpm for 15 min, and the pellet was resuspended in a lysis solution containing 50 mM Tris-HCl, 250 mM NaCl, 2.5% glycerol and 7 mM β- mercaptoethanol (pH 7.8). Resuspended bacteria were sonicated with a Branson digital sonifier, followed by centrifugation at 14,000 rpm for 30 min. The supernatant was collected and incubated with Ni-NTA His•Bind beads (Novagen) in the presence of 10 mM imidazole at 4 °C for 2 hrs. The beads were centrifuged at 2000 rpm for 1 min, collected and washed with 20 volumes of the above lysis solution containing 20 mM imidazole. The protein complex was eluted from the beads with 250 mM imidazole in the lysis solution. Subsequently, the His_6 tag was removed by incubating overnight with thrombin (Sigma) at 20 °C. The protein complex was purified using gel filtration chromatography with a Superose 12 column (GE Healthcare) on a Pharmacia ÄKTA Purifier. The gel filtration solution contained 10 mM HEPES, 150 mM NaCl, 3 mM β-mercaptoethanol and 1% glycerol (pH 7.5). The TRPP2_G833-R872 peptide used for crystallization was expressed in the same expression system and purified with the same protocol. The His_6 tag was cut with thrombin overnight at 20 °C.

Proteins used in pull-down and light scattering experiments were purified either with Ni-NTA His•Bind beads by following the same protocol as above (without gel filtration in pull-down experiments) or with amylose resin (New England Biolabs). When amylose resin was used, a similar protocol was used

except that no imidazole was used and the proteins were eluted with 20 mM maltose. In addition, 5 mM $CaCl_2$ was added in all solutions when purifying the His_6–TRPP2_D732-G928 fragment.

Light scattering measurements. Gel filtration-purified protein samples (at 10-20 mg/ml concentration) were run through a gel filtration column PROTEIN KW-802.5 or KW-804 (Shodex) in a solution containing 150 mM NaCl and 100 mM Tris-HCl (pH 7.5) (for the His_6–TRPP2_D732-G928 fragment, 5 mM $CaCl_2$ was added) and the eluates were examined by static light scattering (Wyatt Technology).

Crystallization and data collection. Crystallization of the TRPP2_G833-G895/PKD1_G4204-R4252 complex and TRPP2_G833-R872 were carried out by using the hanging-drop vapour diffusion method at 20 °C. The volume ratio of protein to reservoir solution in the drop was 1:1. For the TRPP2_G833-G895/PKD1_G4204-R4252 complex, the protein concentration was 10 mg/ml and the reservoir solution contained 20-30 % Dioxane and 100 mM NaAc (pH 4.0-4.4). Only the TRPP2 fragment was in the crystal based on the crystallographic analysis. For TRPP2_G833-R872, the protein concentration was 2 mg/ml and the reservoir solution contained 10% PEG 6000, 1 M LiCl, 100 mM citric Acid, pH 4.0.

Crystals were rinsed in Paratone-N (Hampton Research), and flash-frozen in liquid nitrogen for data collection at 100 K. X-ray diffraction data for the

TRPP2_G833-G895/PKD1_G4204-R4252 complex were collected on a RAXIS-IV detector (Japan) using Cu *K*α radiation (λ=1.5418 Å) from a Rigaku RuH3R X-ray generator. X-ray diffraction data for TRPP2_G833-R872 were collected at the National Synchrotron Light Source (NSLS) beamline X4C on a Mar CCD (λ=0.979 Å). The diffraction images were processed and scaled with the HKL package (7).

Structure determination and refinement. Both structures were determined by the molecular replacement method with the program PHASER (8) using the GCN4 leucine zipper structure (PDB code 1ZIJ) as the search model. The electron density maps were improved using the program ARP/wARP (9), and subsequently more amino acids were built into the new electron density maps with the program COOT (10). Structure refinement was performed with the program CNS (11) and manual adjustments. The final refined models showed excellent stereochemistry, with 100% of the residues within the most favored regions of the Ramachandran plot. Data collection and refinement statistics are summarized in Table S1. All structural graphics were prepared using the program PyMOL (12).

Co-Immunoprecipitation. Cell lystates were obtained as in the cross-linking experiments and were mixed with either monoclonal anti-HA antibody (HA.11) coated beads (Covance) or monoclonal anti-FLAG antibody (M2) coated beads (sigma). After incubation at 4 °C for 2-4 hrs, the beads were spun down and

washed three times with a solution containing 1 X PBS with a total NaCl concentration of 400 mM, 1% DDM and 1/50 (V/V) Protease Inhibitor Cocktail (Sigma). The bound proteins were then eluted by adding 1X SDS sample buffer, incubated at 37 °C for 30 min, and analyzed by SDS-PAGE and Western blot.

Generation of anti-PKD1 serum. Two independent batches of anti-PKD1 serum were produced by GenScript Corporation. The antigen was an 18-amino acid peptide from the N-terminus of mouse PKD1 (EPYLAVYLHSVSQPNEYN, E2931 to N2948), which corresponds to the human sequence used to generate the anti-PKD1 antibody MR3 (13). The peptide was synthesized and conjugated to KLH protein, which was then inject into two New Zealand white rabbits. The resultant anti-sera were tested with ELISA. Both anti-PKD1 sera were tested in our experiments and produced similar results.

Electrophysiology. Perforated-patch recordings were used to record whole-cell currents from HEK 293T cells. For transiently transfected cells, recordings were performed 36-48 hrs after transfection. The standard solution contained 150 mM NaCl, 2.5 mM $CaCl_2$, 10 mM glucose and 10 mM HEPES (pH 7.4). The pipette solution contained 145 mM CsCl, 0.2 mM EGTA, 0.12 mM $CaCl_2$, 10 mM glucose and 10 mM HEPES (pH 7.4). Perforated patches were established by adding 50 μM β-escin in the pipette solution. Pipettes were dipped in escin-free solution and backfilled with escin-containing solution. Pipette resistance ranged from 1.5 to 4 MΩ. Access resistance was monitored untill it dropped below 25 MΩ before

recording started. Series resistance was compensated by 40-80%. Cells were held at -60 mV and 100-ms voltage steps were applied every 2 seconds, ranging from -100 mV to +100 mV in 10 mV increments. Voltage ramps (from -140 mV to +60 mV in 150 ms) were used during serum applications once every 5 seconds. The anti-PKD serum and control serum were used with 25- to 100-fold dilution.

Whole-oocyte currents were recorded with two-electrode voltage-clamp (TEVC). After microinjection with 20 ng/oocyte *of in vitro* synthesized cRNA, oocytes were incubated at 17°C for 4 to 5 days before recording. For recordings of resting currents in a divalent-free solution and of serum-induced currents, the bath solution contained 100 mM NaCl, 2 mM KCl and 10 mM HEPES (pH 7.5). Oocytes were held at -60 mV. For recordings in the presence of a divalent, 2 mM $MgCl_2$ was added to the solution above, and oocytes were held at 0 mV. For resting current recordings, 60 ms long voltage steps from -100 to +100 were applied in 20-mV increments.

Recordings were performed at room temperature.

SI References

1. Shaner, N. C. *et al*. (2004) Improved monomeric red, orange and yellow fluorescent proteins derived from Discosoma sp. red fluorescent protein. *Nat. Biotechnol.* 22:1567-1572.
2. Li, Q. *et al*. (2003) Polycystin-2 Associates with Tropomyosin-1, an Actin Microfilament Component. *J. Mol. Bio*. 325:949-962.

3. Ong, A. C. *et al*. (1999) Polycystin-1 expression in PKD1, early-onset PKD1, and TSC2/PKD1 cystic tissue. *Kidney Int.* 56:1324-1333.

4. Schagger, H. & von Jagow, G (1991) Blue native electrophoresis for isolation of membrane protein complexes in enzymatically active form. *Anal. Biochem.* 199:223-231.

5. Ulbrich MH & Isacoff EY (2007) Subunit counting in membrane-bound proteins. *Nat Methods* 4:319-321.

6. Sonnleitner A, Mannuzzu LM, Terakawa S, & Isacoff EY (2002) Structural rearrangements in single ion channels detected optically in living cells. *Proc Natl Acad Sci U S A* 99:12759-12764.

7. Otwinowski, Z., & Minor, W. (1997) Processing of X-ray diffraction data collected in oscillation mode. *Method Enzymol*. 276:307-326.

8. Storoni LC, McCoy AJ, & Read RJ (2004) Likelihood-enhanced fast rotation functions. *Acta Crystallogr D Biol Crystallogr* 60:432-438.

9. Perrakis A, Morris R, & Lamzin VS (1999) Automated protein model building combined with iterative structure refinement. *Nat Struct Biol* 6:458-463.

10. Emsley P & Cowtan K (2004) Coot: model-building tools for molecular graphics. *Acta Crystallogr D Biol Crystallogr* 60:2126-2132.

11. Brunger AT*, et al.* (1998) Crystallography & NMR system: A new software suite for macromolecular structure determination. *Acta Crystallogr D Biol Crystallogr* 54:905-921.

12. DeLano, W. L. (2002) The PyMOL Molecular Graphics System (DeLano Scientific, Palo Alto, CA), www.pymol.org.

13. Delmas P*, et al.* (2004) Gating of the polycystin ion channel signaling complex in neurons and kidney cells. *Faseb J.* 18:740-742.

SI Figure Legends

Fig. S1. Putative transmembrane topology of PKD1 and TRPP2. The cytoplasmic C termini of both subunits interact directly. It remains to be determined whether PKD1 contains a pore-forming loop between its last two transmembrane segments or elsewhere.

Fig. S2. Distribution of observed EGFP bleaching steps (green bars) for PKD1-mCherry and TRPP2-EGFP dual-fluorescence spots compared to the calculated distribution (white bars) assuming that 4 EGFP molecules exist in each spot. The fit was obtained with the probability of GFP to be fluorescent being set either as a free parameter (*A*) or to 80% (*B*).

Fig. S3. TRPP2-dependent surface expression of PKD1 and PKD1-independent surface expression of TRPP2. (*A*) TIRF image of EGFP and mCherry fluorescence from oocyte expressing PKD1-EGFP and TRPP2-mCherry. Scale bar, 2 μm. (*B*) TIRF image of oocyte expressing PKD1-EGFP. Scale bar, 2 μm. (*C*) TIRF image of oocyte expressing TRPP2-EGFP, showing fluorescent spots that fit the criteria for analysis (green circles). Scale bar, 2 μm. (*D*) Time course of photobleaching of two representative TRPP2-EGFP fluorescence spots showing three EGFP bleaching steps (arrows). (*E*) Distribution of observed and calculated bleaching steps for TRPP2-EGFP fluorescence spots. The 1-3 step distribution is well fit by a binomial distribution (white bars) that assumes that

each spot contains 3 EGFPs and that the probability of EGFP to be fluorescent is 79%.

Fig. S4. Representative overlay of the static light scattering and refractive index chromatograms for the indicated proteins. The measured M.W. for each sample is indicated.

Fig. S5. Stereo view of the electron density map contoured at 1.0σ for the N terminal part of the TRPP2 coiled coil domain trimer structure. Only a monomer is shown here.

Fig. S6. The mut6 mutation abolishes the surface expression of TRPP2. TIRF image of EGFP fluorescence from oocyte expressing TRPP2-EGFP (*A*) or TRPP2_mut6-EGFP (*B*). Image of TRPP2-EGFP is a duplication of Fig. S3*C* without the green circles. Scale bar, 2 μm.

Fig. S7. Homomeric TRPP2 complexes and heteromeric TRPP2/PKD1 complexes do not produce spontaneous (resting) currents in HEK 293T cells and *Xenopus* oocytes. Our results contradict those of two previous studies reporting the functional expression of TRPP2 in oocytes (Vassilev et al., 2001) and of PKD1 and TRPP2 in a mammalian cell line (Hanaoka et al., 2000).
(A) Resting whole-cell currents recorded at -100 mV and +100 mV from untransfected 293T cells, PKD- and TRPP2-transfected cells, TRPP2-transfected

293T cells stably-expressing PKD1 (PKD1 stable cell), and PKD1 stable cells. Membrane potential was clamped in 100 ms steps (10-mV increments) between -100 mV and +100 mV from a holding potential of -60 mV. There was no significant statistical difference in current amplitude among the four groups of cells tested, except that the PKD1 stable cells showed smaller inward current at -100 mV.

(B) Representative current-voltage relationship (I-V curve) of the resting currents recorded from untransfected cells and TRPP2-transfected PKD1 stable cells. The I-V curves are very similar to each other and to those reported by Hanaoka et al. (2000).

(C) Resting whole-oocyte currents recorded at -100 mV and +100 mV by two electrode voltage clamp (TEVC) in a divalent-free bath solution from *Xenopus* oocytes injected with the cRNA of the indicated constructs. 60-ms voltage steps from -100 mV to +100 mV were applied in 20 mV increments from a holding potential of 0 mV. Although a current was observed in PKD1- and TRPP2-injected oocytes that was absent in water-injected oocytes, this current was also present in oocytes injected with all other indicated constructs. Since PKD1 and TRPP2_mut6 do not reach the surface membrane when expressed alone or together (see the main text), we conclude that this current is not produced by channels formed by PKD1 and/or TRPP2; instead, injection of the PKD1 and/or TRPP2 cRNA probably induces an endogenous current. Data in this figure were obtained from blind experiments.

(D) Representative I-V curves of whole-oocyte currents in a divalent-free bath solution for oocytes injected with the indicated cRNAs.

(E) Resting whole-oocyte currents recorded at -100 mV and +100 mV by TEVC in a both solution containing 2 mM Mg^{2+} from *Xenopus* oocytes injected with the cRNA of the indicated constructs. 100-ms voltage steps between -100 mV and +100 were applied in 20-mV increments from a holding potential of 0 mV. A large outward current was observed in oocytes injected with PKD1 and TRPP2, with PKD1 alone, and with PKD1 and TRPP2_mut6, but not in oocytes injected with water, TRPP2 or TRPP2_mut6. Thus, we conclude that this current is induced by PKD1. Our findings are consistent with a previously reported current induced in oocytes by expressing the carboxyl-terminal fragment of PKD1 (Vandorpe et al., 2001).

(F) Representative I-V curves of whole-oocyte currents in Mg^{2+}-containing bath solutions for oocytes injected with PKD1 or a chimeric PKD1 mutant named PKD1wP2S6. In PKD1wP2S6, the last (i.e. 11^{th}) putative transmembrane segment (TM11) was replaced by the putative pore-forming TM6 of TRPP2. The I-V curves were obtained in a Na^+ bath solution or in an $NMDG^+$ bath solution. Notice that the I-V curves are very similar between WT PKD1 and PKD1wP2S6 in both solutions. In this set of experiments, our goal was to examine whether the PKD1-induced current in (E) was conducted by a channel whose pore is either wholly or partly formed by PKD1. Six PKD1 mutants that contained different mutations in its putative pore region between TM10 and TM11 were tested. The mutants were: PKD1_D4043A/T4044A, PKD1_L4053-G4058A (all

six amino acids between L4053 and G4058 were mutated to alanine), PKD1_P4062A/T4063A, PKD1_E4068A/S4069A, PKD1wP2S6 (as mentioned above), and PKD1wP2pore (in the region between TM10 and TM11 of PKD1 was replaced by the region between TM5 and TM6 of TRPP2). Our expectation was that if the current shown in (E) was conducted by channels whose pore is either wholly or partly formed by PKD1, some of the mutations will abolish this current (by destroying the pore) or alter the ion selectivity (e.g. changing the permeability to $NMDG^+$). The results showed that all six PKD1 mutants were still capable of inducing the same current as shown in (E) and that they all show very similar permeability to Na^+, Cs^+ and $NMDG^+$. These results lead us to conclude that most likely the currents shown in (E) are conducted by channels formed by endogenous oocyte proteins, whose expression is stimulated by PKD1 cRNA injection. These channels seem to be different from those that mediate the currents in (C).

Altogether, the results shown in this figure indicate that TRPP2 and/or PKD1 do not produce spontaneously active surface channels when expressed in HEK 293T cells and *Xenopus* oocytes. Our results also caution against ascribing resting currents induced by the expression of either or both constructs in these systems to channels formed by either or both proteins.

References for Fig. S7.

Vassilev PM, *et al.* (2001) Polycystin-2 is a novel cation channel implicated in defective intracellular Ca^{2+} homeostasis in polycystic kidney disease. *Biochem Biophys Res Commun* 282:341-350.

Hanaoka K*, et al.* (2000) Co-assembly of polycystin-1 and -2 produces unique cation-permeable currents. *Nature* 408:990-994.

Vandorpe DH, *et al.* (2001) The cytoplasmic C-terminal fragment of polycystin-1 regulates a Ca2+-permeable cation channel. *J Biol Chem.* 276:4093-101.

Fig. S8. Serum-induced whole-cell currents in HEK 293T cells and *Xenopus* oocytes expressing PKD1 and/or TRPP2. It has been shown that the TRPP2/PKD1 complex can be activated by an anti-PKD1 antibody named MR3 (Delmas et al., 2004). MR3 was raised against an epitope (E2939-N2956) in human PKD1 in an N terminal extracellular region near the receptor for the egg jelly domain (Delmas et al., 2004). Since we failed to record spontaneously active currents from homomeric TRPP2 complexes and heteromeric TRPP2/PKD1 complexes, we attempted to obtain stimulus-induced currents from these complexes. We generated two separate batches of anit-mouse PKD1 serum by using a synthesized peptide (EPYLAVYLHSVSQPNEYN, E2931 to N2948 from mouse PKD1) as the epitope. This antigen peptide corresponds to the human sequence that was used to generate MR3 (Delmas et al., 2004).
(A) Time course of current activation by an anti-PKD1 serum or a control rabbit serum in HEK 293T cells stably-expressing both PKD1 and TRPP2 (PKD1/TRPP2 stable line), or transiently transfected with TRPP2_mut6 (TRPP2_mut6 tansfected). The anti-PKD1 serum evoked a current in PKD1/TRPP2 stable cells (left) and TRPP2_mut6 transfected cells (middle); however, the control serum also induced a current of similar amplitude in

PKD1/TRPP2 stable cells (right) and in TRPP2_mut6 tansfected cells (not shown). Currents were recorded at -140 mV.

(B) Representative I-V curves of the currents shown in (A).

(C) Comparison of the current density at -140 mV of anti-PKD1 serum- or control serum-induced currents in the indicated HEK 293T cells. Results were obtained from blind as well as non-blind experiments, as indicated. There was large variation in the current response in most of the cell types. No significant difference was found among the cells tested. The observation that the anti-PKD1 serum evoked a current in cells not expressing exogenous PKD1 (such as TRPP2 stable cells and TRPP2 transfected cells) suggests that these currents are not caused by the activation of PKD1. Furthermore, the observation that the control serum induced a current in PKD1/TRPP2 stable cells suggests that an active compound other than the anti-PKD1 antibody in the serum is able to activate this current. Finally, the observation that the anti-PKD1 serum was still capable of evoking a current in TRPP2_ΔD643/E648/E650/E651, in which four negatively charged amino acids in the putative pore-forming region were deleted, suggests that this current is not conducted by the PKD1/TRPP2 complex.

(D) Time course of current activation by an anit-PKD1 serum or a control serum in *Xenopus* oocyte injected with PKD1 and TRPP2 or with water. Currents were recorded at -60 mV. The observation that this current could be induced by the control serum as well as the anit-PKD1 serum in water-injected oocytes indicate that the current is not conducted by the PKD1/TRPP2 complex.

Taken together, these results indicate that the anti-PKD1 sera we obtained cannot activate the PKD1/TRPP2 complex. They also indicate that an unknown compound in the rabbit serum is able to activate an endogenous channel in HEK 293T cells and *Xenopus* oocytes.

Reference for Fig. S8.

Delmas P*, et al.* (2004) Gating of the polycystin ion channel signaling complex in neurons and kidney cells. *Faseb J* 18:740-742.

Table S1. Data collection and refinement statistics

Data collection		
Crystal	TRPP2_G833-G895	TRPP2_G833-R872
Space group	*R*32	$P6_3$
Cell dimensions		
a, b, c (Å)	43.6, 43.6, 200.4	32.4, 32.4. 70.3
α, β, γ (°)	90, 90, 120	90, 90, 120
Resolution (Å) *	1.90 (1.97-1.90)	1.90 (1.97-1.90)
Wavelength (Å)	1.5418	0.97927
R_{merge} (%)†	6.8 (28.7)	5.2 (22.8)
Mean $I/\sigma I$	36.2 (9.93)	32.8 (5.1)
Completeness (%)	100 (100)	98.7 (92.9)
Redundancy	10.7 (10.6)	5.7 (3.4)
Refinement		
Resolution (Å)	1.9	1.9
No. reflections	5883	2991
R_{work} / R_{free} (%)‡	19.9/25.9	19.5/22.7
No. atoms		
Protein	505	300
Water	110	32
B-factors		
Protein	25.8	25.0
Water	38.6	39.9
R.m.s. deviations		
Bond lengths (Å)	0.014	0.012
Bond angles (°)	1.3	1.2

*Values in parentheses are for the highest-resolution shell.

† $R_{merge} = \Sigma_h\Sigma_i|I_{hi} - \langle I_h\rangle|/\Sigma_h\Sigma_i I_{hi}$

‡ $R = \Sigma_h||F_o| - |F_c||/\Sigma_h|F_o|$

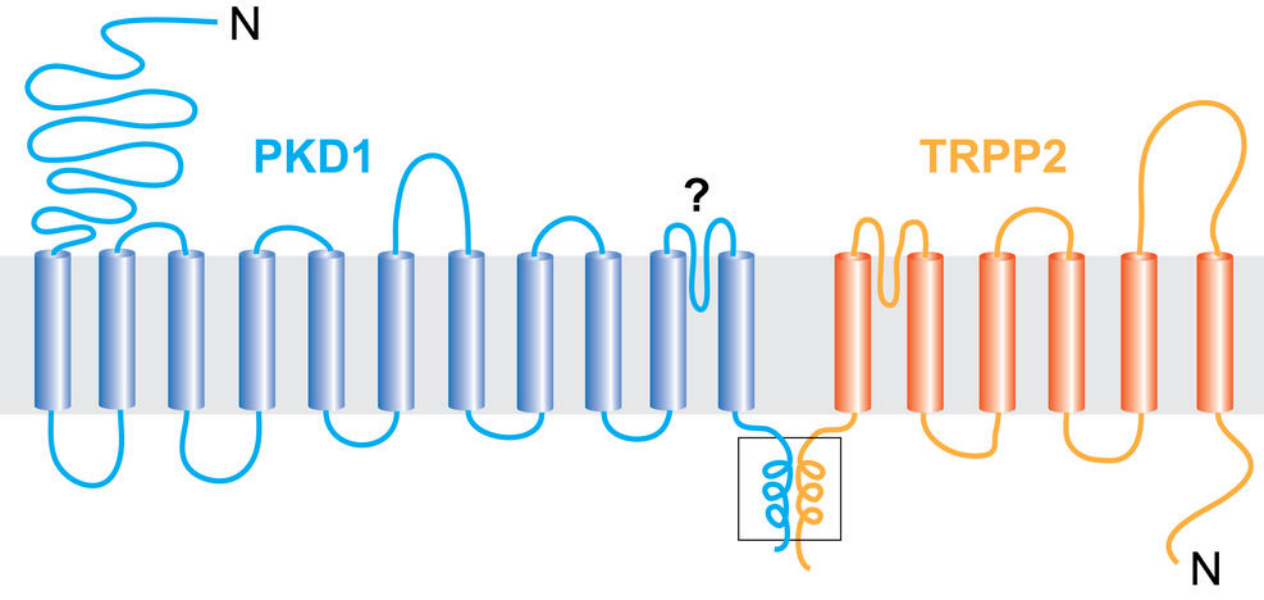
N
PKD1
?
TRPP2
N

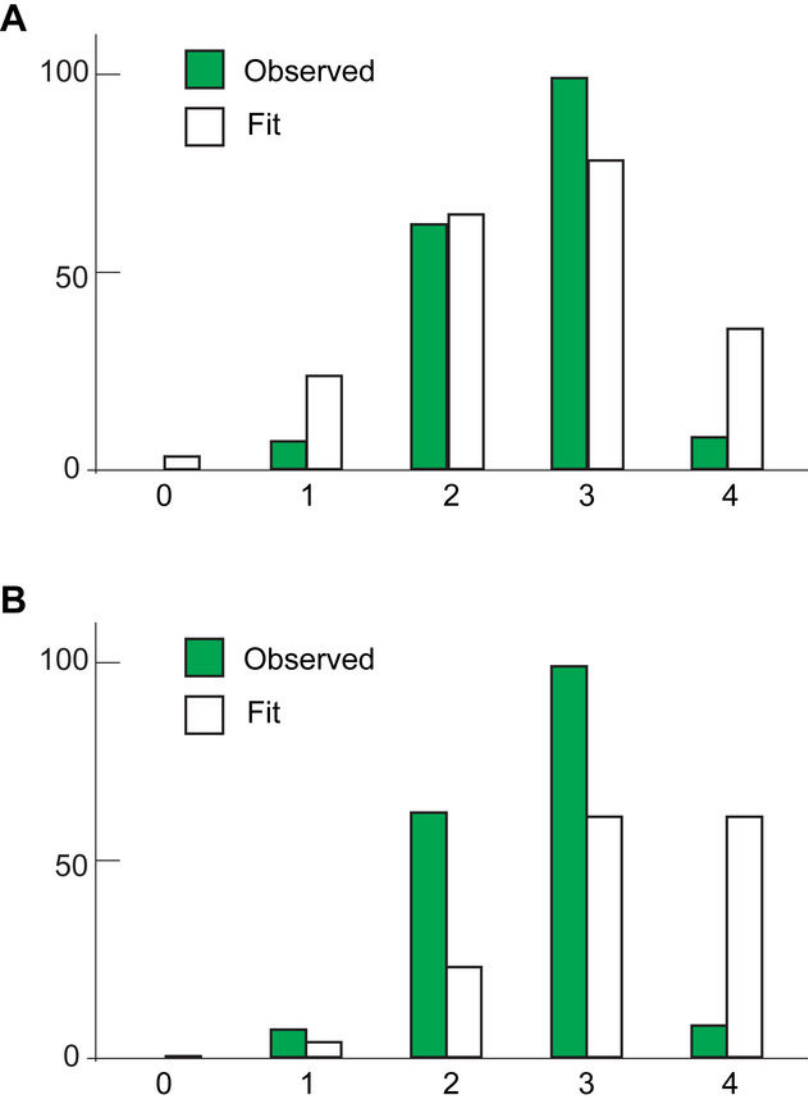
A
100
50
0
Observed
Fit
0
1
2
3
4
B
100
50
0
Observed
Fit
0
1
2
3
4

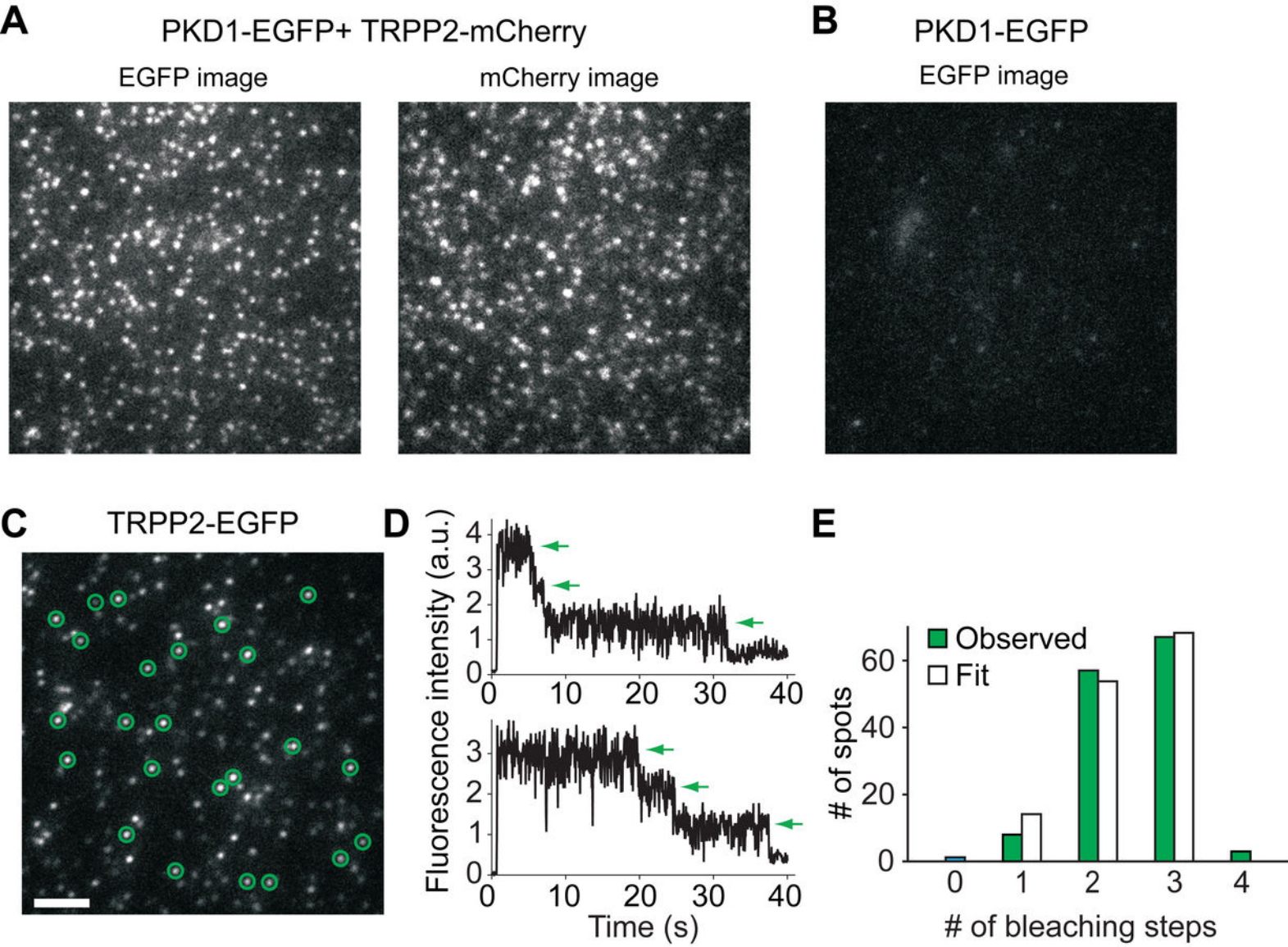
A
PKD1-EGFP+ TRPP2-mCherry
EGFP image
mCherry image
B
PKD1-EGFP
EGFP image
C
TRPP2-EGFP
D
Fluorescence intensity (a.u.)
Time (s)
E
Observed
Fit
# of spots
# of bleaching steps

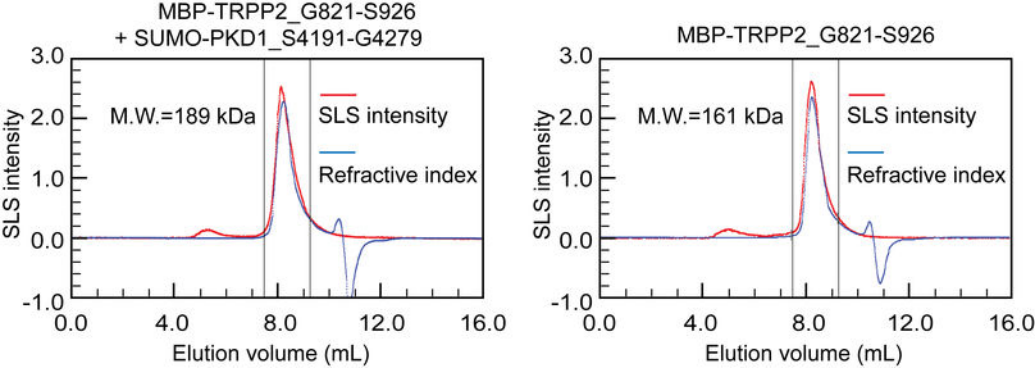
MBP-TRPP2_G821-S926
+ SUMO-PKD1_S4191-G4279
M.W.=189 kDa
SLS intensity
Refractive index
SLS intensity
Elution volume (mL)
3.0
2.0
1.0
0.0
-1.0
0.0
4.0
8.0
12.0
16.0
MBP-TRPP2_G821-S926
M.W.=161 kDa
SLS intensity
Refractive index
SLS intensity
Elution volume (mL)

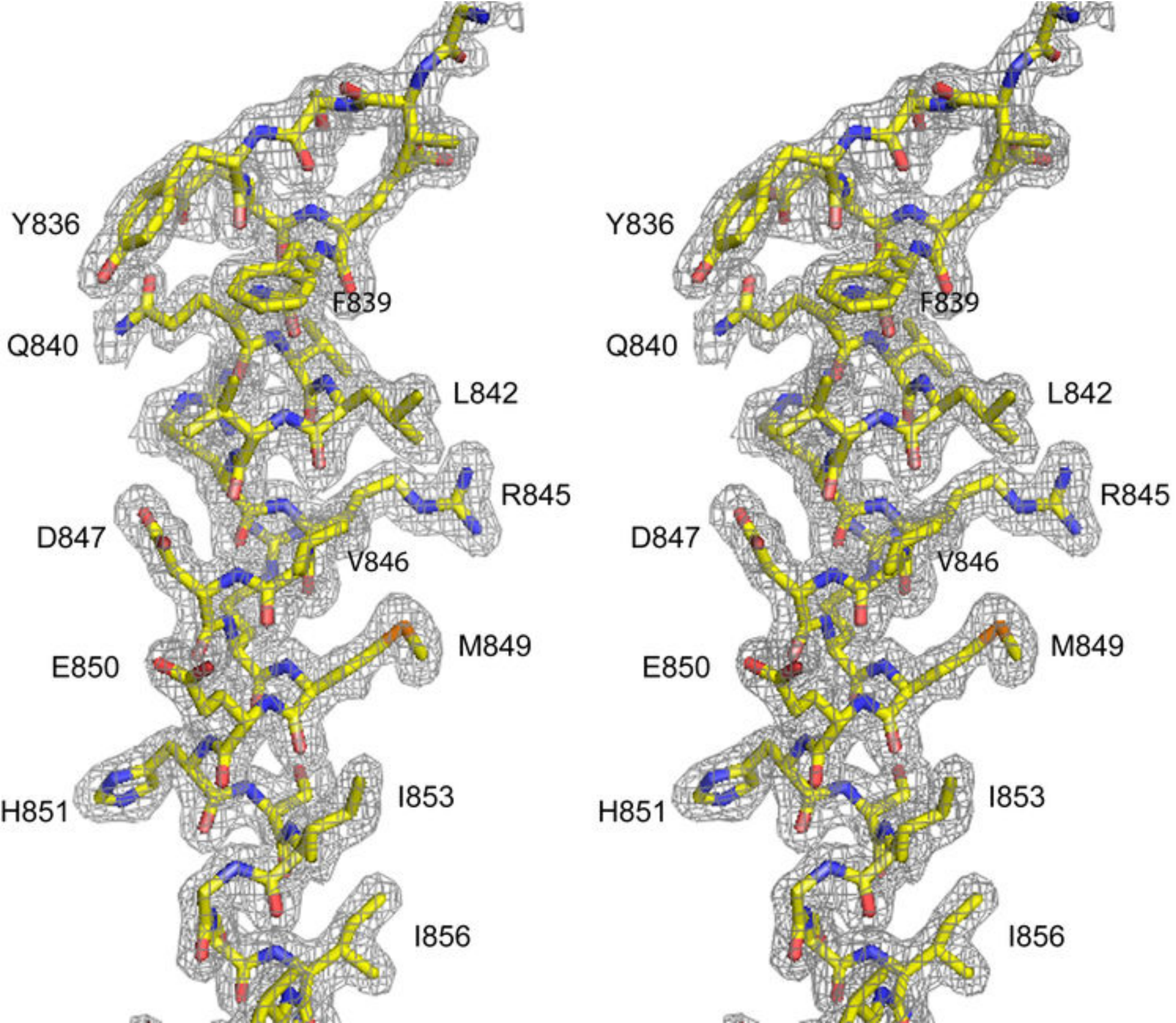
Y836
F839
Q840
L842
R845
D847
V846
M849
E850
H851
I853
I856
Y836
F839
Q840
L842
R845
D847
V846
M849
E850
H851
I853
I856

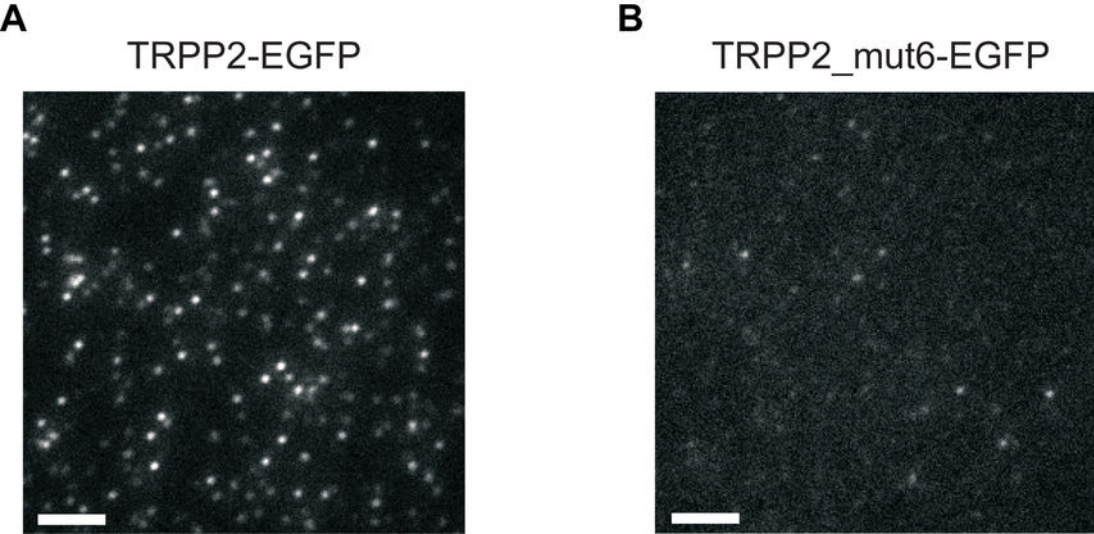
A
TRPP2-EGFP
B
TRPP2_mut6-EGFP

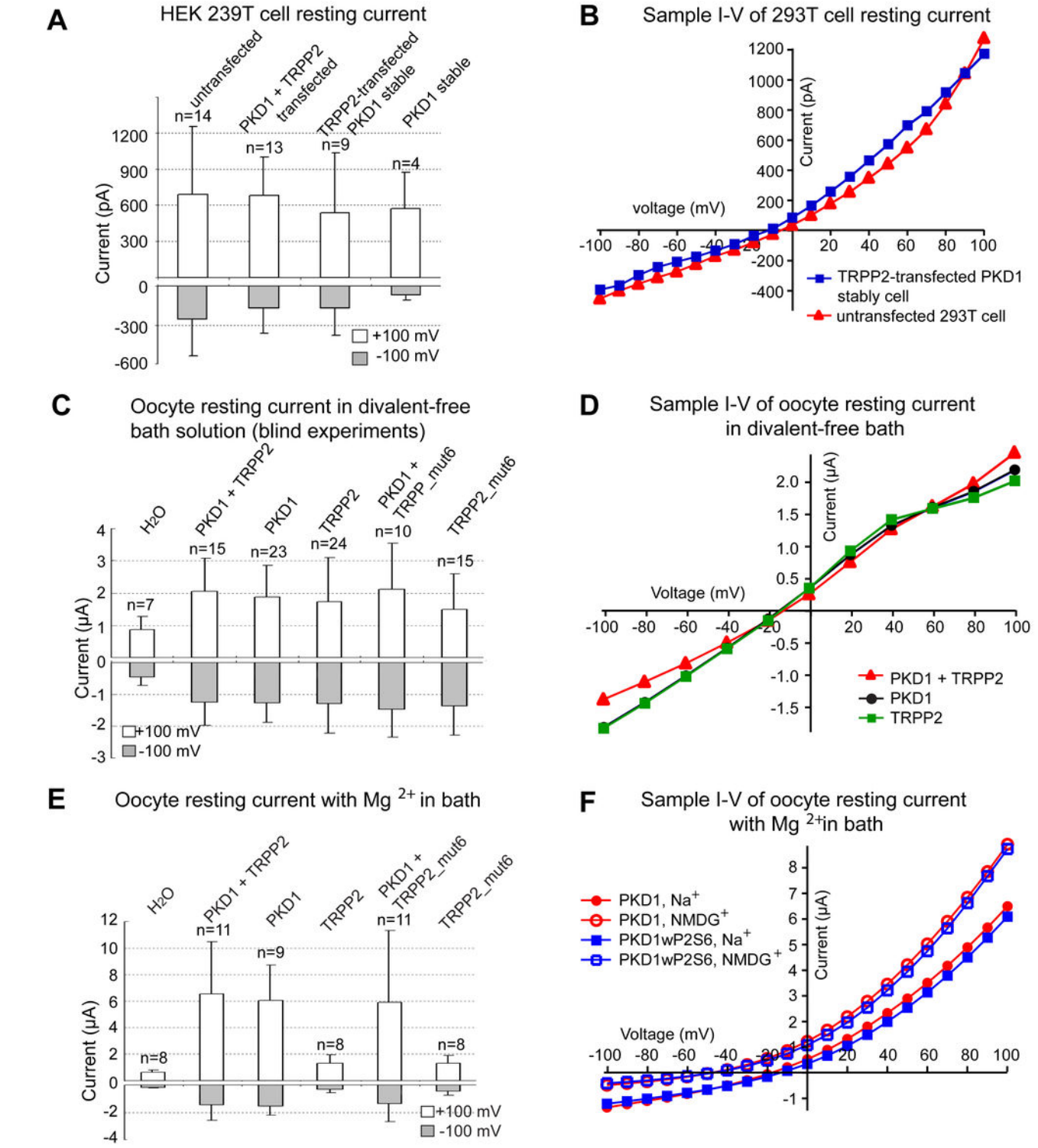
A
HEK 239T cell resting current
untransfected
PKD1 + TRPP2 transfected
TRPP2-transfected PKD1 stable
PKD1 stable
n=14
n=13
n=9
n=4
Current (pA)
+100 mV
-100 mV
B
Sample I-V of 293T cell resting current
Current (pA)
voltage (mV)
TRPP2-transfected PKD1 stably cell
untransfected 293T cell
C
Oocyte resting current in divalent-free bath solution (blind experiments)
H2O
PKD1 + TRPP2
PKD1
TRPP2
PKD1 + TRPP_mut6
TRPP2_mut6
n=7
n=15
n=23
n=24
n=10
n=15
Current (μA)
+100 mV
-100 mV
D
Sample I-V of oocyte resting current in divalent-free bath
Current (μA)
Voltage (mV)
PKD1 + TRPP2
PKD1
TRPP2
E
Oocyte resting current with Mg 2+ in bath
H2O
PKD1 + TRPP2
PKD1
TRPP2
PKD1 + TRPP2_mut6
TRPP2_mut6
n=8
n=11
n=9
n=8
n=11
n=8
Current (μA)
+100 mV
-100 mV
F
Sample I-V of oocyte resting current with Mg 2+in bath
PKD1, Na+
PKD1, NMDG+
PKD1wP2S6, Na+
PKD1wP2S6, NMDG+
Current (μA)
Voltage (mV)

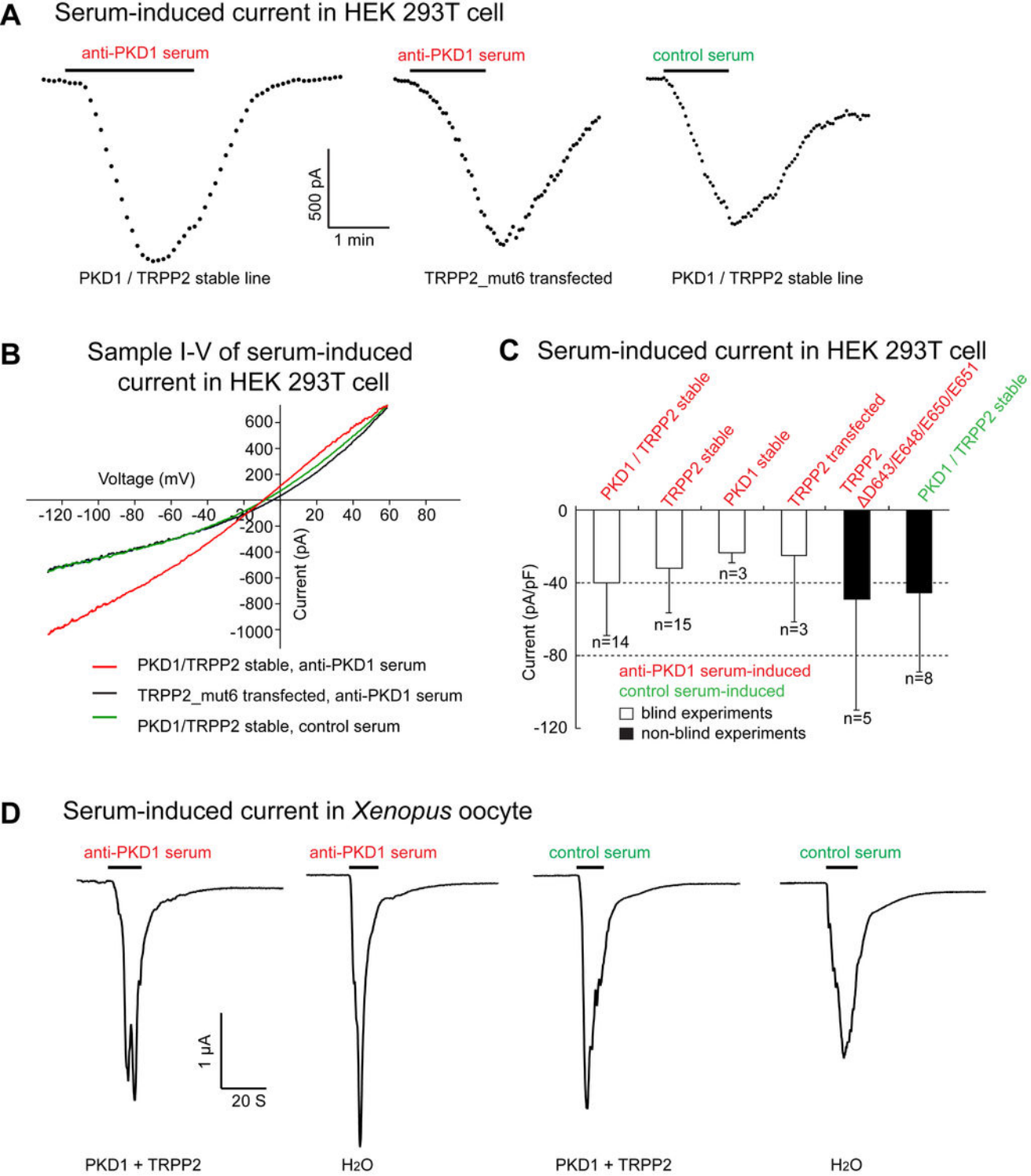
A
Serum-induced current in HEK 293T cell
anti-PKD1 serum
anti-PKD1 serum
control serum
500 pA
1 min
PKD1 / TRPP2 stable line
TRPP2_mut6 transfected
PKD1 / TRPP2 stable line
B
Sample I-V of serum-induced current in HEK 293T cell
Voltage (mV)
Current (pA)
PKD1/TRPP2 stable, anti-PKD1 serum
TRPP2_mut6 transfected, anti-PKD1 serum
PKD1/TRPP2 stable, control serum
C
Serum-induced current in HEK 293T cell
PKD1 / TRPP2 stable
TRPP2 stable
PKD1 stable
TRPP2 transfected
TRPP2 ΔD643/E648/E650/E651
PKD1 / TRPP2 stable
Current (pA/pF)
n=14
n=15
n=3
n=3
n=5
n=8
anti-PKD1 serum-induced
control serum-induced
blind experiments
non-blind experiments
D
Serum-induced current in Xenopus oocyte
anti-PKD1 serum
anti-PKD1 serum
control serum
control serum
1 μA
20 S
PKD1 + TRPP2
H2O
PKD1 + TRPP2
H2O